ADE 951 297

TECHNICAL REPORT -RD-ST-88-9

AD-A204 051

MODAL ANALYSIS AND TESTING OF MISSILE SYSTEMS

Larry C. Mixon
John A. Schaeffel, Jr.
Peter L. Green
1LT Roque L. Salas
Russell Garner
Structures Directorate
Research, Development, and Engineering Center

DECEMBER 1988

U.S. ARMY MISSILE COMMAND
Redstone Arsenal, Alabama   35898-5000

DTIC
ELECTE
FEB 1 5 1989
S   D
H

89 2 14 001

REPORT DOCUMENTATION PAGE

Form Approved
OMB No 0704-0188
Exp Date Jun 30. 198

1a REPORT SECURITY CLASSIFICATION	1b RESTRICTIVE MARKINGS
Unclassified	

2a. SECURITY CLASSIFICATION AUTHORITY	3. DISTRIBUTION / AVAILABILITY OF REPORT
2b. DECLASSIFICATION / DOWNGRADING SCHEDULE	Distribution A. Approved for public release; distribution is unlimited.

4 PERFORMING ORGANIZATION REPORT NUMBER(S)	5. MONITORING ORGANIZATION REPORT NUMBER(S)
TR-RD-ST-88-9	

6a. NAME OF PERFORMING ORGANIZATION	6b. OFFICE SYMBOL (If applicable)	7a. NAME OF MONITORING ORGANIZATION
Structures Directorate Res, Dev, and Engr Ctr	AMSMI-RD-ST	

6c. ADDRESS (City, State, and ZIP Code)	7b. ADDRESS (City, State, and ZIP Code)
Commander, US Army Missile Command ATTN: AMSMI-RD-ST Redstone Arsenal, AL 35898-5247	

8a. NAME OF FUNDING / SPONSORING ORGANIZATION	8b. OFFICE SYMBOL (If applicable)	9. PROCUREMENT INSTRUMENT IDENTIFICATION NUMBER

8c. ADDRESS (City, State, and ZIP Code)	10. SOURCE OF FUNDING NUMBERS			
	PROGRAM ELEMENT NO.	PROJECT NO	TASK NO	WORK UNIT ACCESSION N

11. TITLE (Include Security Classification)

MODAL ANALYSIS AND TESTING OF MISSILE SYSTEMS

12. PERSONAL AUTHOR(S)
Larry C. Mixon, John A. Schaeffel, Jr., Peter L. Green, 1LT Roque L. Salas, Russell Garner

13a. TYPE OF REPORT	13b. TIME COVERED	14. DATE OF REPORT (Year, Month, Day)	15. PAGE COUNT
Summary	FROM _____ TO Sep 88	December 1988	77

16. SUPPLEMENTARY NOTATION

17.	COSATI CODES		18. SUBJECT TERMS (Continue on reverse if necessary and identify by block number)
FIELD	GROUP	SUB-GROUP	Modal modal shapes
			eigenvectors FEMS
			eigenvalues

19. ABSTRACT (Continue on reverse if necessary and identify by block number)

This study was performed to establish the effectiveness of using modal tests to verify th accuracy of NASTRAN Finite Element Models (FEMs) of missiles. The structure used in this study was a mock-up of the FOG-M system. While the missile was not a flight version, the structural characteristics and internal subcomponents were sufficiently close to the FOG-to allow meaningful conclusions concerning the testing and analysis techniques. The stud also permitted a comparison between two different methods of testing, i.e., normal mode a random response. Also, sensitivity analyses were conducted on the NASTRAN mathematical model to identify peculiarities associated with a subroutine used to compute eigenvectors and eigenvalues and to study the requirement for additional nodes when modeling the wings and fins. Eight modes of vibration were measured and correlated with the FEM models. Excellent to good correlation was obtained for the critical first bending modes of the airframe, wings, and fins. Excellent to good correlation was obtained for the wings and fins higher mode shapes, but differences in most frequencies were noted for the higher mod of vibration. (continued)

20. DISTRIBUTION / AVAILABILITY OF ABSTRACT	21 ABSTRACT SECURITY CLASSIFICATION
☐ UNCLASSIFIED/UNLIMITED ☒ SAME AS RPT. ☐ DTIC USERS	Unclassified

22a. NAME OF RESPONSIBLE INDIVIDUAL	22b TELEPHONE (Include Area Code)	22c OFFICE SYMBOL
Dr. Larry C. Mixon	(205) 876-6157	AMSMI-RD-ST

DD FORM 1473, 84 MAR

83 APR edition may be used until exhausted.
All other editions are obsolete.

BLOCK 19 (con't):   A Lessons Learned Chapter is provided that documents
                    all difficulties experienced, and suggestions were
                    provided for future test and analysis efforts. Finally,
                    recommendations are offered on how this effort can most
                    effectively be extended to a flight model of the FOG-M.

TABLE OF CONTENTS

LIST OF ILLUSTRATIONS

LIST OF ILLUSTRATIONS (con't)

LIST OF ILLUSTRATIONS (con't)

LIST OF TABLES

I. INTRODUCTION

This study was performed to investigate and document the effectiveness of using experimental modal testing to verify the adequacy of Finite Element Models (FEMs) of complex missile structures. Before pursuing the stated objective, the more encompassing question of "Why FEMs?" was addressed. Insight was gained by examining the advantages that FEMs offer in the structural design and development of guided missiles. Basically, missile airframes and supporting hardware are designed to withstand quasi-steady-state loads (static loads) and then tested and modified until the structures withstand the dynamic loads associated with real world deployment:

A. Static Loads

The structural designs of many missiles are based primarily on the quasi-steady state forces or the use of static accelerations, g's, for the inertia loadings. The aerodynamic, propulsive (internal pressure and thrust), and resulting inertia loads (propulsive and maneuvering) are considered static forces. Even the most dynamic of loads are sometimes approximated with "equivalent static accelerations" such as the use of eight g's static to simulate the loads imparted to a missile and its launcher when a helicopter crashes. A diagram of the more recent development of the FOG-M structure is shown in Figure 1. Even this simplified or truncated design approach can be enhanced using FEMs early in the development process.

Initially, simple beam models should be used in the formulation of the mathematical models with limited use of plate and shell elements. Once the models are established, the quasi-steady-state or static forces can be applied to the multinodes, and the internal moment and shear forces derived for detailed stress analysis. If more sophisticated depiction of internal stresses and deflections are needed, more detailed mathematical models can be formulated using plate, shell, and solid elements such as six node triangles and eight node quadrilaterals. Once the adequacy of the simplified model has been established as a baseline, the extension of these results to more sophisticated models is straightforward.
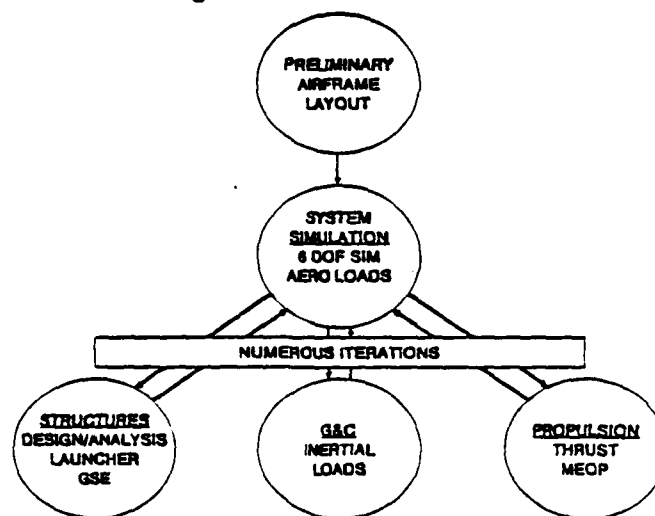
Figure 1. Quasi-steady state force analysis approach.

B. Dynamic Forces

The use of FEMs becomes imperative if dynamic loads are used in the analysis. The basic disciplines are well established to include the dynamic forces and the related structural responses early in the design process. The prudent approach is to use these tools which will significantly reduce costly redesigns, engineering change proposals, and hardware retrofits, and yield more efficient structures earlier in the development sequence. The design and development process will remain iterative as prototype hardware becomes available and the testing of actual hardware is possible. The difference in the structural designs is based on actual loads and not in oversimplified static assumptions.

Typical missile dynamic loads include the following:

- -shock and vibration resulting from handling, transportation, and missile launch platform dynamics such as those contributed by helicopters and ground vehicles.

- -launch dynamics

- -impacts associated with vehicle incidents such as the previously discussed helicopter crashes

- -blade induced oscillations from helicopter and fixed wing aircraft

- -oscillatory thrust force

- -buffeting

- -acoustical excitation

- -structural response resulting from thrusters

- -aerodynamic force resulting from missile flexibility or aeroelasticity

These dynamic loads do occur in real life. But, in the "static load" design process, the stresses associated with the loads are hidden in the safety factors and/or margins of safety that appear in the stress analysis. In cases where these margins are not sufficient to cover the ignored dynamic loads, the faulty designs are discovered later when failures occur during testing or in field use. In many cases, the dynamic or dynamic related responses are actually the loads that ultimately control the design of the missile. Unfortunately, the loads are considered later in the development process and control the redesign in the last review. As shown in Figure 2, after the basic development process is complete, flight tests, ground transportation tests, and laboratory tests are used to identify structural problems resulting from dynamic forcing functions. These structural problems are corrected and an iterative process follows redesigning, fabricating, and testing with continual modification throughout the life of the missile system.

2

UNKNOWNS

- LAUNCH DYNAMICS
- SHOCK & VIBRATION FROM
  HANDLING, TRANSPORTATION,
  & LAUNCH PLATFORMS
- IMPACT RESPONSE
- AERODYNAMIC AND ACOUSTICAL
  BLADE INDUCED FORCES
- OSCILLATORY THRUST
- THRUSTERS
- BUFFETING

AIRFRAME LAUNCHER/ TRANSPORTER

FLIGHT TESTS

ACCELEROMETERS STRAIN GAGES

LAB TESTS

MIL STD 810D OR FLIGHT/ROAD TEST DATA

ROAD TESTS

ACCELEROMETERS
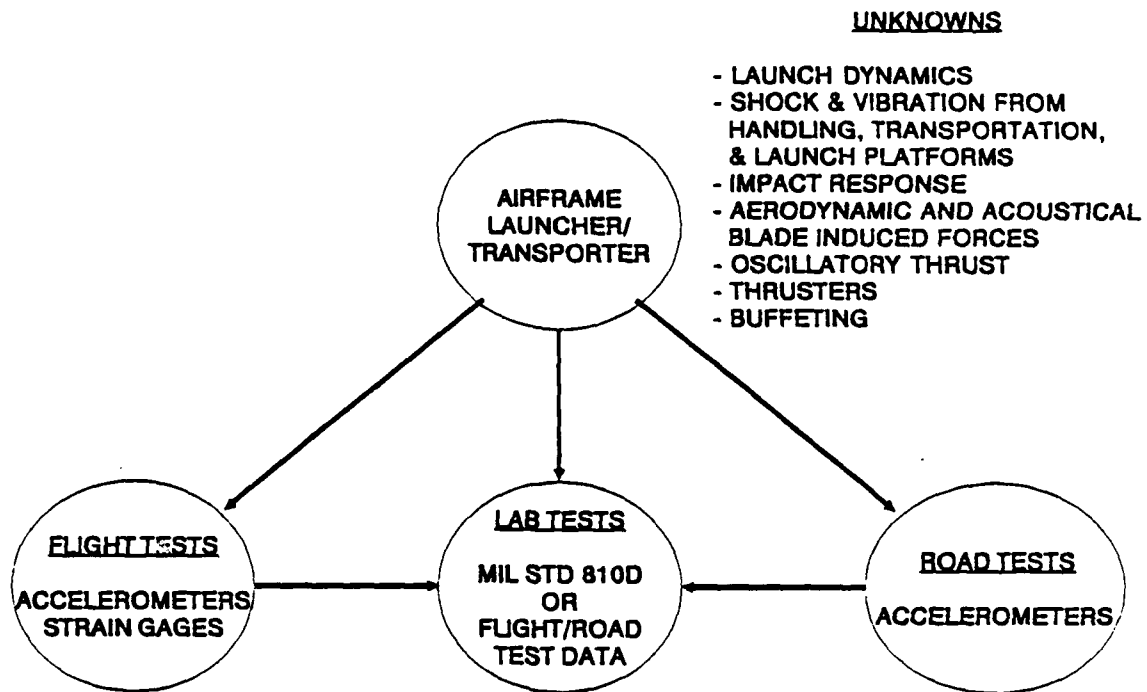
Figure 2. Dynamic force test approach.

C. Modal Analysis and Testing

The need for adequate mathematical models has been established which substantiates the basic argument for using FEMs. The stated purpose of this study is to establish that good engineering correlation can be obtained between the FEM predicted modes of vibration and the results from laboratory modal tests. Correlation between predicted and measured modes of vibration establishes the basic validity of the models. In addition, verification of the modes proves that the section properties and mass distributions are correct. Static load and deflection tests can and should be used in the establishment of material section properties. However, the modal analysis and testing approach carries this process one step further in that mass distribution is included in the process. Also, the importance of structural features such as nonlinear joints and structural damping are an inherent part of the modal analysis process.

3

In addition to verification of the mathematical models, the modal analysis and testing serve a significant role in the following analyses:

Free Flight Rockets — identification of structural damping which controls coupling between roll, pitch, and yaw

— aeroelasticity studies for the long L/D low frequency missiles

Guides Missiles — separation of structural frequencies from guidance and control loops

— identification of ideal bulkhead location for seeker and gyro mounting

— identification of actuator locations

D. Missile Under Study

A prototype missile structure of the FOG-M is used in this study. In addition to providing the demonstration of correlation between a mathematical model prediction and testing, this study provides a comparison between the more classical normal mode testing technique and the now more popular random vibration approach. Also, observations are offered concerning the strong points and shortcomings of the two test techniques. Finally, Lessons Learned in the performance of this study are provided for future consideration.

II. MISSILE AIRFRAME ANALYSIS

A. Body Normal Mode Measurements

Two accelerometers were first placed at positions 1 and 2 shown in Figure 3 with the exciter coupled to the bottom of the missile directly below accelerometer position 2. Results are shown in Figure 4 with the major resonances being 283.6 Hz at location 1 and 132.6 Hz at location 2. The axes of these plots are linear peak g's versus frequencies from 15 to 500 Hz. Also note, the minor resonances that fall between 85 and 95 Hz for both locations which will be shown later as resonances associated with other subsystems internal to the missile.

Figure 5 shows a repeat of the first sine sweep (Figure 4 data) which shows acceptable repeatability. The cross-hair must be aligned with one of the resonances. This alignment was arbitrarily selected as 131.4 Hz for accelerometer 2. As shown, the cross-hair indicates a shift for the same resonance at accelerometer location 1 (bottom plot). This shift is within the resolution of this instrumentation system. The shift represents a difference of 3 to 4 percent from the indicated frequency of 131.4 Hz.

Next, the transducer located at position 1 was moved to location 3 and the sine sweep repeated. The driving acceleration was somewhat less as shown by comparing location 2 peak g's on Figure 4 and Figure 6 but is within acceptable tolerances. The lower frequency, 128.4 Hz, (same resonance as the 131.4 Hz previously noted) was again evident at locations 2 and 3 and a second resonance of 289.7 Hz was prevalent at location 3 which is close to the 283.6 Hz observed during the first test.

The last sine sweep test conducted was with a transducer at location 2 and a moveable accelerometer at location 4 on the inside lip of the cantilevered fiber optics spool. The results are shown in Figure 7 with the only predominant resonance at location 4 being at approximately 92 Hz. Additional measurements at various locations along the length of the spool would have been helpful but would have necessitated disassembly of the structure. Other measurements were made on the outer skin at the approximate location of the base of the spool, and accelerations were small. Consequently, it is safe to infer that the first cantilever mode for the spool is 92 Hz.

Now, recall the resonance observed on the front portion of the missile at a frequency between 85 and 95 Hz. An earlier modal experiment was conducted on the TV seeker and gimbal mounting and is documented in Reference 1. The first resonance of the cantilever TV seeker was found to be between 95 and 105 Hz. The exact gimbal system and seeker were probably a later version than the system examined in this study, but the range of the frequencies strongly suggests that both resonances are cantilevered beam modes of the mounted seeker. During these more recent tests, the missile was not disassembled, but it appears conservative to assume that the first cantilever mode of the seeker is approximately 90 Hz.

The next step in the normal mode measurement scheme was to conduct dwell tests at the frequencies identified in the sine sweep tests. The exciter was placed in exactly the same position as for the sine sweep test. One of the two available accelerometers was specified as the fixed stationary reference to ensure the same relative accelerometer is being applied for each test setup and to establish phase relationships for the measurements. In these measurements, the reference accelerometers were place above the excitation source or location 5 in Figure 8. Also shown on this figure are the nine locations for the roving accelerometers. The driving force is then set at a frequency near the resonances identified earlier and limited frequency sweeps are run up and down to pinpoint the resonance to be studied. The first resonance was between 128.4 Hz and 132.6 Hz from the sine sweep tests depending on location of the measurement. In the case of these limited frequency sweeps, the resonant frequency was identified as 130.3 Hz or between the previous measurements. Once this measurement scheme was established, data were recorded in a format similar to the first four columns of Table 1.

TABLE 1. Airframe First Body Bending
FREQUENCY = 130.3 Hz

LOC	AMP	REF AMP	PHASE	$COS(\phi_1-\phi_2)$	SHAPE
1	.507	.738	-158.9	+ .99	+ .50
2	.221	.753	-140.0	+ .98	+ .22
3	.349	.751	4.6	- .92	- .32
4	.659	.748	3.6	- .91	- .60
5	.688	.738	2.8	- .91	- .63
6	.595	.729	- 5.5	- .84	- .50
7	.517	.747	- 16.9	- .71	- .37
8	.342	.753	- 81.7	+ .33	+ .11
9	1.390	.794	0	+1.00	+1.00

Next, the maximum acceleration was identified which was at location 9 for this particular frequency. Then, the cosine of the angle between the maximum acceleration and the phase angle at each of the other eight locations was computed with the results shown in column 5 of the table. Next, the eight remaining acceleration measurements were normalized to the maximum acceleration and multiplied by the cosine of the phase angle differences. This product becomes the mode shape. This final mode shape will be shown later after a discussion of the NASTRAN modal predictions.

This same procedure was then repeated for the second noted resonance which was around 283.6 Hz to 289.7 Hz from the sine sweep tests. The limited frequency sweep yielded a resonance of 280.0 Hz again between the earlier measurements. The sine dwell tests yield the data in Table 2 which again will be shown in graphical format after the following discussion on the NASTRAN modal predictions.

TABLE 2.   Airframe Second Body Bending
FREQUENCY = 280.0 Hz

LOC	AMP	REC AMP	PHASE	$\cos(\phi_1 - \phi_2)$	SHAPE
1	.697	.404	-133.0	+ .74	+ .24
2	.376	.414	-110.0	+ .41	+ .07
3	.326	.414	- 53.0	- .54	- .08
4	.361	.417	- 16.6	- .93	- .16
5	.418	.416	- .5	-1.0	- .20
6	.419	.417	+ 1.0	-1.0	- .19
7	.381	.417	- 3.2	- .99	- .18
8	.153	.419	- 69.8	- .27	- .02
9	2.110	.416	-175.5	+1.0	+1.00
*	.375		-169.0		
**	.495		-155.0		

* right side vertical direction location 9
** bottom side vertical direction location 9

B.   NASTRAN Modal Analysis

A beam model for the FOG-M is shown in Figure 9. When three dimensional modal plots are obtained from the NASTRAN plotting routines, it is extremely difficult to ascertain the higher frequency body bending modes because the relatively low frequency wings (20 Hz range) and fins bending modes (45 Hz range) are extremely flexible and the displacements are normalized to the wings and fins even though the mode of vibration is primary body bending. An illustration of this point is shown in Figure 10 which is a plot of the NASTRAN 16th mode in only the x-z plane. Even though the mode is primarily body bending, the wing and fin displacement overshadow the displacements of interest. This observation is even more prevalent when trying to interpret three dimensional NASTRAN mode plots.

7

In order to resolve the NASTRAN predicted bending modes for the body bending from those of the wings and fins, the mathematical model was then recomputed with the wings and fins totally removed and then with lumped masses in place of the appendages at the junctures with the missile body. Also, hand calculations were made using average section properties and assuming equally distributed mass for a simple free-free beam for the case when the wings and fins are removed. Results are shown in Figure 11 and the following table:

TABLE 3. Calculated First Body Bending

CONDITION	FREQUENCY
First body bending w/o wings & fins manual calculations	167.3 Hz
First body bending w/o wings & fins NASTRAN	160.8 Hz
First body bending lumped wing & fin masses NASTRAN	144.7 Hz
First body bending distributed wing & fin masses NASTRAN	147.2 Hz
Second body bending distributed wing & fin masses	467.77 Hz

This exercise provided confidence that the NASTRAN mathematical model is approximately correct and the modes have been correctly identified when masked by the large displacement associated with the lower frequency wing and fin modes of vibration. Now that the background has been provided on the mathematical model, the comparison of NASTRAN modal predictions and the measurements made using the normal modal analysis scheme can continue.

C. Comparison Measurements ; id NASTRAN Modal Analysis

Figure 12 shows comparison of the predicted and measured first mode of vibration. The NASTRAN data was extracted from the computer printout, only the body bending was plotted and the data renormalized to the maximum peak for the body elements. Excellent correlation was obtained for the mode shape which leaves little doubt that the correct modes are being compared. Obviously, a discrepancy exists between the predicted and measured frequencies, i.e., 147 Hz predicted and 130 Hz measured. One possible source of error in the mathematical model is the numerous structural joints in the missile. There are seven structural joints in the FOG-M missile body. Each of these joints can introduce flexibility not in the basic shell from the following:

-bolt(s) bending
-deflection in shell due to beam bending
-beam deflection
-deflection due to clearances (slop)

A possible refinement to the mathematical model in missile body simulation would be to add additional elements for the joints and study the effect on modal predictions. This refinement or others are necessary if the difference between 130 and 147 Hz is unacceptable.

The second measured resonance was 260 Hz. A plot of the measured mode shape and the NASTRAN second mode of vibration is shown in Figure 13. This mode is definitely not the actual second mode and occurs at a frequency significantly below what would be expected based on a first mode of 130 Hz. The second mode should be at a frequency which is approximately two and three quarters to three times the lower frequency or 358 to 390 Hz. This observation is further substantiated by the fact that the vertical vibration was also measured on one side and on the bottom of the missile as shown in Table 2. The magnitude was significantly less, indicating that missile body bending was not taking place. This resonance is attributed to some localized deflections and is not of significant importance in understanding the overall response of thé missile.

9

III. WING(S) ANALYSIS.

A. Left Wing Normal Mode Measurements

The FOG-M has four wings. The configuration chosen for this modal test was to position one set of wings horizonally. The left wing refers to the left-hand side when facing the direction of the forward motion of the missile. The configuration tested actually had three wings since the bottom wing was removed so the exciter could be positioned closer to the center line of the wing. As will be shown later, all three wings could have been measured simultaneously at each identified modal frequency. This sequence would have been directly comparable to that used for the NASTRAN modal predictions. However, available instrumentation and time suggest another approach. The same information can be gained from the less time consuming task of measuring one wing. This is the approach followed in this series of tests except that in addition to the left wing which is free of voids, cutouts, etc., the right wing was measured separately to study the effect of a cutout in the top of the wing. The cutout is used to show internal moving wing parts such as springs and rods in the mock-up missile. A schematic of the top view of the missile is shown in Figure 14. The electrodynamic shaker is also shown in the figure placed directly beneath the missile and connected to the underside of the missile with a short rod or stinger. A tapped hole in a bulkhead of the missile body conveniently accepted the stinger.

The sequence was to again conduct sine sweeps over the frequency bands of interest. The results from these sine sweeps are shown in Figure 15 (15 to 200 Hz), Figure 16 (150 to 400 Hz), and Figure 17 (350 to 500 Hz). The top curve in each figure is the accelerometer located on the tip of the wing (position 1) and the bottom plot on each figure is the accelerometer located at the base of the wing (position 6). Examination of these plots shows the major resonances to be 20 Hz, 173 Hz, 191 Hz, and 506 Hz (not shown). Each one of the resonances was then investigated in detail as presented in the following paragraphs.

The resonances were again isolated by conducting limited frequency band sweeps near the indicated frequencies until the peak response was isolated. The first resonance, 19.6 Hz, data are given in Table 4, and the mode plot provided in Figure 18 with the predicted NASTRAN modal frequency and shape. Almost perfect correlation was obtained between the NASTRAN mode shape and the measured modal response.

TABLE 4. Left Wing First Bending Mode
FREQUENCY = 19.6 Hz.

LOC	AMP	REF AMP	PHASE	$\cos(\phi_1-\phi_2)$	SHAPE
1(tip)	2.90	.29	-144.6	+1.00	+1.00
2	2.00	.28	-141.0	+1.00	+ .69
3	1.30	.29	-139.0	+1.00	+ .45
4	.83	.28	-131.0	+ .97	+ .28
5	.36	.31	-112.0	+ .84	+ .10
6(base)	.22	.28	- 25.0	- .49	- .04

The next two modes measured were second mode bending modes of 175 and 192 Hz. The measured mode shapes are given in Tables 5 and 6. A graphical comparison of the two modes is given in Figure 19 which shows both modes to be second mode beam bending. Next, these two measured modes are plotted versus the NASTRAN mode shapes in Figures 20 and 21.

TABLE 5. Left Wing Second Bending Mode
FREQUENCY = 175 Hz

LOC	AMP	REF AMP	PHASE	$\cos(\phi_1-\phi_2)$	SHAPE
1(tip)	9.40	.29	65.0	- .96	- .90
2	2.70	.28	-71.0	+ .48	+ .13
3	9.80	.34	233.0	+1.00	+ .98
4	10.00	.38	228.0	+1.00	+1.00
5	5.60	.30	249.0	+ .93	+ .52
6(base)	.39	.28	-41.0	- .02	0

TABLE 6. Left Wing Second Bending
FREQUENCY = 192 Hz

LOC	AMP	REF AMP	PHASE	$\cos(\phi_1-\phi_2)$	SHAPE
1(tip)	7.30	.41	33.5	+1.00	+1.00
2	1.80	.30	- 93.0	- .59	- .15
3	6.30	.40	215.0	-1.00	- .86
4	6.50	.43	209.0	-1.00	- .89
5	4.60	.31	237.0	- .92	- .58
6(base)	.29	.28	- 15.0	+ .66	+ .03

Again, good correlation was obtained as to mode shapes. However, the frequencies do not agree. The theoretical frequencies were 90 Hz, 119 Hz, 119 Hz, and 120 Hz. See Figure 22 for predicted mode shapes. There are four frequencies because of the four wings which provide four coupled eigenvectors and eigenvalues for each mode. Again, the two measured frequencies for this one wing were 175 and 192 Hz.

The first candidate source that could explain the difference between measured and predicted higher bending mode frequencies is the fixity at the base of the wings and the flexibility of the missile body in the region of the wing(s) attachment. The model could be modified to include torsional springs and/or simulants for nonlinear effects in an attempt to raise the NASTRAN higher mode frequencies while not significantly modifying the first bending mode. This provided excellent correlation for both frequency and mode shape. Another possible explanation for the higher frequency difference could be the mass distribution used in the models of the wings. The mass of the internal working parts of the wings was distributed along the wing which would tend to lower the predicted natural frequencies.

11

The additional modeling refinements are not warranted for the majority of missile analyses. The displacements which control strains/stresses are a function of frequency squared. The ratio of the squares of the first and second measured modes for the wings is 19.62/1752 or 1.25 percent. The Power Spectral Density (PSD) levels for the vast majority of the vibration environments (forcing functions) actually decrease in magnitude (g2/Hz) at the higher frequencies (see Reference 2). This observation is readily understood when the natural frequency of the carrier vehicle and mounting structure is taken into consideration. Typically, the suspension system will be in the lower frequency range; consequently, a reduction in vibration energy at the higher frequencies should be expected. Also, the transportation and missile delivery platform vibrations are more severe than flight vibrations such as acoustic and buffeting. The ground based environments control the structural design for vibrations.

The last measured wing mode was located at 506 Hz and the measured values are given in Table 7. The measured mode shape and NASTRAN prediction are given in Figure 23. Just as with the second bending mode, good mode shape correlation was obtained, but a wider dispersion between measured and predicted frequencies was obtained, e.g., 506 Hz measured with the four predicted frequencies falling between 278 and 319 Hz. Since the second bending mode frequency did not agree, even a lesser degree of agreement is expected when comparing frequencies for the third bending mode. The previously mentioned differences in fixity and mass distributions could explain the difference in frequencies.

TABLE 7. Left Wing Third Bending Mode
FREQUENCY = 506 Hz

LOC	AMP	REF AMP	PHASE	$\cos(\phi_1-\phi_2)$	SHAPE
1(tip)	6.30	.46	-120.0	+ .99	+ .52
2	7.70	.54	16.0	- .82	- .53
3	.79	.50	-240.0	- .36	- .02
4	6.30	.50	-110.0	+ .95	+ .50
5	11.90	.40	-129.0	+1.00	+1.00
6(base)	.77	.54	- 6.6	- .54	- .03

B. **Left Wing Random Mode Measurements.**

The procedure for conducting the random modal measurements is given in Reference 3. In summary, the procedure calls for exciting the structure with random white noise (flat spectrum) energy and recording the measurements for use in subsequent analyses. The preferred technique to isolate which frequencies to study is to measure the ratio of the accelerometer of interest and the input force in units of g's/lbf. Plots for the six positions defined in Figure 14 are given in Figures 24 through 29. In this format, the identification of which natural frequencies to study is difficult; consequently, the equipment manufacturer provides a code called "find mode" which provides a weighted average of the g's/lbf for all locations under consideration. This presentation for the frequency band from 15 to 210 Hz is given in Figure 30. The predominant frequencies for this band are 21, 173, and 195 Hz which provide excellent agreement with values measured using the normal mode method. In addition, the first and second beam bending mode shapes show acceptable agreement with the previous modal survey technique (see Figures 31, 32, and 33). Unfortunately, other frequencies shown in Figure 30 might also warrant study. For example, the fourth highest amplitude is approximately 119 Hz. The software has no method to differentiate good modes from nonmodes of other parts of the missile resonating such as internal missile components. This lack of ability to differentiate good from superfluous modes is amplified when the next step is taken in the software to measure the mode shape. Figure 34 shows a mode plot of the 119-120 Hz frequency. The mode appears to be that of a pinned-pinned beam and not of the cantilevered wing. Assuming that the signal is out of the noise, two sources could explain this apparent mode. First, the measurement scheme was designed to measure beam bending with the accelerometers located along the center line of the symmetrical wing. The mode could be an artifact of the first torsional mode which should fall between 100 and 200 Hz with the first beam bending mode of 20 Hz. Placement of accelerometers in a matrix along the plane of the wing would have allowed for the identification of torsional modes. This modeling/test program was initiated as a simple NASTRAN beam model approach; consequently, modeling and measuring the torsional modes of vibration were out of scope of the project. Another explanation of the 120 Hz mode is that some other component, missile substructure, appendage, etc., is vibrating and the resulting wing mode shape falls between the first and second beam bending modes. In the future, great care should be taken to ensure that actual modes are being measured and not artifacts of other natural resonances when using the Random Mode Measurements technique. The slower Normal Mode Measurements method requires that each apparent mode of vibration be identified and verified as a predominate structural mode as the tester/analyst moves up the frequency scale.

C. **Right Wing Normal Mode Measurements.**

The right wing normal modes were measured by the same procedure previously described for the left wing. The locations of accelerometers and the electrodynamic shaker are given in Figure 35. The primary differences between the right wing and left wing are the presence of the previously described cutout and a longer rod or stinger to attach the shaker to the missile. The sine sweep data are given in Figure 36 (15 Hz to 200 Hz), Figure 37 (150 Hz to 400 Hz), and Figure 38 (350 Hz to 600 Hz). The identified resonant frequencies are 21 Hz, 160 Hz, 433 Hz, and 481 Hz.

13

As with the other missile substructures, sine dwell tests were conducted at these frequencies. The data are given in Table 8 for the 21 Hz mode, and the cantilevered beam mode shape is provided in Figure 39. Again, excellent correlation is provided for the left wing first mode both with data from the normal mode method and the random mode method, and with the NASTRAN model mode predictions.

TABLE 8. Right Wing First Bending Mode
FREQUENCY = 21.0 Hz

LOC	AMP	REF AMP	PHASE	$\cos(\phi_1 - \phi_2)$	SHAPE
1(tip)	2.50	.26	-167.0	+1.00	+1.00
2	1.62	.23	-167.0	+1.00	+ .65
3	1.08	.22	-166.0	+1.00	+ .43
4	.52	.21	-164.0	+1.00	+ .21
5	.13	.20	-140.0	+ .89	+ .05
6(base)	.17	.21	- 9.0	- .93	- .06

The second indicated mode from the sweep tests was a strong mode at 160 Hz. The dwell tabulated data are given in Table 9 and plots in Figure 40. This is definitely one of the second beam bending modes. The frequency is lower than the lowest measured comparable mode for the left wing of 175 Hz. Of course, both the 160 and 175 Hz measured frequencies are higher than the NASTRAN model prediction of 90 Hz. The differences between the frequencies of right and left wing second bending modes are probably due to the effect of the cutout. If this is true, some calibration is provided as to what could be expected when using modal testing to study composite structure defects. The mode shapes for the right and left wings are similar, but the frequencies are different, i.e., 160 Hz versus 175 Hz. The effect of the cutout is detectable; however, the relative size of the defect (cutout) is large compared to the wing plan form area. These observations provide some insight into using modal testing to detect flaws in composite structures. Future investigators should give attention to the second and higher modes of vibration when studying internal flaws.

TABLE 9. Right Wing Second Bending Mode
FREQUENCY = 160 Hz

LOC	AMP	REF AMP	PHASE	$\cos(\phi_1 - \phi_2)$	SHAPE
1(tip)	6.11	.35	+ 41.0	+1.00	-1.00
2	2.01	.32	+243.0	- .93	+ .31
3	5.90	.35	+228.0	- .99	+ .96
4	4.75	.36	+208.0	- .97	+ .75
5	3.95	.30	+250.0	- .87	+ .56
6(base)	.27	.31	- 21.0	+ .47	- .02

Minor responses were observed at 172 and 214 Hz in the sine sweep data. The relative magnitudes are insufficient to indicate major bending modes of vibration.

The last two modes to be studied on the right wing were modes located at 433 Hz and 481 Hz. Tabulated data are given in Tables 10 and 11, and the mode plots are provided in Figures 41 and 42. The modes appear to be approaching the third beam mode measured on the left wing which was a classical third bending mode at 506 Hz. The poor definition of the right wing mode shape is probably again due to the cutout. The defect evidently has more influence at the higher modes.

TABLE 10. Right Wing Bending Mode
FREQUENCY = 433 Hz

LOC	AMP	REF AMP	PHASE	$\cos(\phi_1-\phi_2)$	SHAPE
1(tip)	5.10	2.20	+ 90.0	- .92	- .47
2	10.00	1.20	- 67.0	+1.00	+1.00
3	4.70	1.40	- 6.0	+ .48	+ .23
4	3.50	1.40	+ 5.0	+ .31	+ .11
5	6.50	1.20	+ 19.0	+ .70	+ .46

TABLE 11. Right Wing Bending Mode
FREQUENCY = 481 Hz

LOC	AMP	REF AMP	PHASE	$\cos(\phi_1-\phi_2)$	SHAPE
1(tip)	5.80	.71	+160.0	- .87	- .34
2	14.80	.95	+ 9.8	+1.00	+1.00
3	5.60	.89	+158.0	- .85	- .32
4	2.58	.88	+267.0	- .22	- .04
5	2.37	.72	+239.0	- .65	- .10
6(base)	.66	1.00	+ 72.0	+ .47	+ .02

IV. FIN(S) ANALYSIS.

The four fins were connected to the missile structure via linkages, pins, actuators, and other hardware. These structures contained a significant amount of clearance (slop). During flight, these mechanisms were energized with pneumatic pressure and the greater portion of these nonlinearities were eliminated. One approach to these tests would have been to apply the applicable pressures and to pin or fix any remaining joints that might introduce excessive clearance. During these particular tests, a simplified approach was followed where two fins were connected to either side of a .625 inch cube block. The cube block was connected to the exciter with a stinger (small diameter threaded rod) and a force transducer. A schematic of the test setup is shown in Figure 43. The length of the rod connecting the fins to the cube block was .191 inch which is representative of the length in the actual missile application and is the same length chosen in the NASTRAN math model. Again, normal mode measurements and random response techniques were used to identify the modes of vibrations for comparison to NASTRAN predictions.

A. Fin Normal Mode Y-Z Direction.

The first normal mode measurements were made in the Y-Z directions. A plot of the sine sweep data is shown in Figure 44. The vertical axis depicts transmissibility, that is, the acceleration at the right hand tip (accelerometer 1) divided by the acceleration at the top of the cube mounting block. As given in the figure, the highest amplitude resonances were 42, 291, 320, and 470 Hz. Next, each of these resonances were studied in detail. Limited band frequency sweeps were conducted at a nominal 42 Hz frequency and the peak response frequency was established to be 43 Hz. Dwell tests were then conducted and the results are given in Table 12 and Figure 45.

TABLE 12. Fin First Bending Mode
FREQUENCY = 43 Hz

LOC	AMP	REF AMP	PHASE	$\cos(\phi_1 - \phi_2)$	SHAPE
1(tip)	10.37	.84	-127.0	+1.00	+1.00
2	8.40	.60	- 92.0	+ .81	+ .66
3	5.99	.61	- 67.0	+ .50	+ .29
4	4.04	.63	- 57.0	+ .34	+ .13
5	1.97	.64	- 52.0	+ .25	+ .05
6(base)	.71	.64	- 14.0	- .39	- .03

Also shown on Figure 45 is the NASTRAN predicted mode of 43 Hz. Both the frequency and modes shape correlations are considered acceptable. The model could be changed to provide exact correlation if desired. The next three resonances studied were 294, 320, and 328 Hz which bracket the two second bending modes of the fins. Tables 13, 14, and 15 summarize these data.

TABLE 13.   Fin Second Bending Mode
FREQUENCY = 294 Hz

LOC	AMP	REF AMP	PHASE	$\cos(\phi_1-\phi_2)$	SHAPE
1(tip)	10.54	1.94	+126.2	+1.00	+1.00
2	2.09	2.07	+144.9	+ .95	+ .19
3	2.36	2.07	- 8.3	- .70	- .16
4	5.33	2.02	- 14.3	- .77	- .39
5	4.92	2.03	- 12.1	- .75	- .35
6(base)	3.07	2.05	- 5.1	- .66	- .19

TABLE 14.   Fin Second Bending Mode
FREQUENCY = 320 Hz

LOC	AMP	REF AMP	PHASE	$\cos(\phi_1-\phi_2)$	SHAPE
1(tip)	13.78	2.22	+ 72.7	+1.00	+1.00
2	.95	2.13	+117.5	+ .71	+ .05
3	5.47	1.93	- 32.1	- .26	- .10
4	8.89	2.00	- 50.3	- .54	- .35
5	8.50	1.90	- 35.7	- .32	- .20
6(base)	3.64	1.95	-16.90	+ .01	+ .00

TABLE 15.   Fin Second Bending Mode
FREQUENCY = 328 Hz

LOC	AMP	REF AMP	PHASE	$\cos(\phi_1-\phi_2)$	SHAPE
1(tip)	13.50	2.30	+ 62.5	+1.00	+1.00
2	3.79	1.94	+105.8	+ .72	+ .20
3	5.22	1.87	- 63.9	- .56	- .22
4	10.01	1.94	- 78.5	- .78	- .58
5	7.51	1.79	- 51.2	- .40	- .22
6(base)	3.07	1.81	- 24.3	+ .06	+ .01

The mode shapes are shown in Figure 46 and all three modes appear to be the second bending mode. Since two fins are being tested as one structure, two second bending modes should be expected. The presence of three modes in the frequency band of 294 to 328 Hz can be explained by slight differences in the fins which were of different vintage and probably different internal structures. Also, small differences existed in the short (nominal .191 inch) cantilever rods for each fin. The two frequencies of 294 and 328 Hz were selected for comparison with NASTRAN predictions. This comparison is shown in Figure 47. Again, acceptable correlation between measured and predicted modal frequencies and shapes was achieved.

The last Y-Z direction mode to be measured with this technique and with the fins in this orientation was located at 482 Hz. The tabulated data is as follows:

TABLE 16.   Fin Bending Mode
FREQUENCY = 482 Hz

LOC	AMP	REF AMP	PHASE	$COS(\phi_1-\phi_2)$	SHAPE
1(tip)	13.87	2.70	+ 39.8	+1.00	+1.00
2	1.04	1.60	- 54.3	- .07	- .01
3	13.35	2.30	+220.6	-1.00	- .96
4	12.75	2.07	+227.7	- .99	- .91
5	2.57	1.88	- 18.5	+ .52	+ .10
6(base)	1.30	1.40	+ 23.3	+ .95	+ .09

A plot of this mode shape is shown in Figure 48. The mode appears to resemble a second bending mode except for the relatively low vibration levels near the base of the fin. Due to the separation of frequency from the previously described second bending modes in the 300 Hz frequency range and the low base node amplitudes, this mode was classified as a localized effect probably due to the short rod section used to cantilever the fins.

B.   Fin Random Response Y-Z Direction.

The fins were retested in the same direction except the random response technique was used to identify the modes of vibration. The frequency response is shown in Figure 49. The frequencies readily identified were 42.5, 305, 326, and 494 Hz. Additional acceleration locations were used during these measurements. As shown in the first random mode plot, Figure 50, measurements were made at 11 locations with position 1 being the fin tip and position 11 being the top of the .650 inch cube block used to cantilever the fins. This plot again clearly showed the first mode in the weak axis to be 46 Hz. The NASTRAN prediction was not repeated since the correlation was excellent when compared to the previously described normal mode data.

The mode shapes for the 300 Hz frequency range resonances are shown in Figures 51 and 52. The resonances located at 306 and 326 Hz are the second bending modes. These modal frequencies were found to be 294 and 328 Hz when measured by the normal mode method which is again excellent correlation between the two techniques. Note, 21 measurements were made using the random response approach so both fins could be studied simultaneously.

The last frequency studied during this series of tests was located at 490 Hz (see Figure 53) which was the same resonance studied at 482 Hz in the normal mode technique. Only the right fin was studied. Exactly the same minimal response of the nodes near the base is apparent as previously discussed, and again this resonance appeared to be associated with vibration of the outer portion of the fin with the cantilever rod remaining essentially stationary. As discussed in the missile airframe body bending analysis, the structure atempted

to approach the mode shape of the closest predominant mode of vibration even when a subset of the structure or subcomponent was in a resonant condition.

C. **Fin Normal Mode X Direction.**

The fins were rotated 90 degrees to permit the identification of the longitudinal or X direction modes of vibration. The sine sweep plot for the right fin is shown in Figure 54. The vertical axis is the tip acceleration divided by the acceleration at the base of the fin immediately to the right of the cantilever rod. One extreme, almost classical, resonance is indicated at at 81 Hz. Subsequent dwell tests pinpointed the frequency to be 82 Hz as given in Table 17 and Figure 55. The flexibility was provided by the short rod used to cantilever the fins with the body of the fins essentially acting as a rigid mass.

TABLE 17. Fin First Bending Mode X-Direction
FREQUENCY = 82 Hz

LOC	AMP	REF AMP	PHASE	$\cos(o_1-o_2)$	SHAPE
1(tip)	12.90	1.06	-130.0	+1.00	+1.00
2	10.20	.78	-133.0	+1.00	+ .79
3	7.60	.50	-117.0	+ .97	+ .57
4	5.30	.38	- 88.0	+ .74	+ .30
5	3.10	.38	- 82.0	+ .67	+ .16
6(base)	1.20	.38	- 63.0	+ .39	+ .04

D. **Fin Random Response X-Direction.**

The frequency response function is shown in Figure 56 with the one resonance indicated at 83 Hz. Subsequent mode measurements were conducted at 82 Hz and are given in Figure 57. Again, excellent correlation was provided between the normal mode and random response measurement techniques.

V. NASTRAN FINITE ELEMENT MODEL SENSITIVITY ANALYSIS.

Discussion of the NASTRAN analysis has been limited in the preceding Chapters and only the final results have been presented. Actually, numerous iterations were made of the basic beam model prior to, during, and subsequent to the testing. In one case, retesting both statically and dynamically was accomplished to better understand the results and to improve correlation. This sensitivity analysis is important because it demonstrates some peculiarities of the modal extraction code used in this version of NASTRAN and some considerations that should be given such analysis and test programs in the future.

A summary is given in Table 18. Seven NASTRAN models were studied not counting the special models used to identify the body bending modes discussed in detail in Chapter II. Model 1 was the basic model and was used for the comparisons between predicted and measured modes except for the fins. This model is considered the baseline. Note, the first wing bending modes had three frequencies (modes) and not the expected four associated with four wings. Four modes are given for the fin(s) first bending mode and all higher frequency bending modes for both the wing(s) and fin(s).

Model 2 is a repeat of the first model, but the lower wing was removed as accomplished in the actual test sequence. The number of first bending modes reduced to two and the higher wing modes dropped to the appropriate number of three. A slight shift in frequencies was noted.
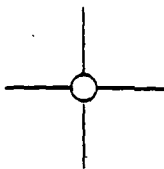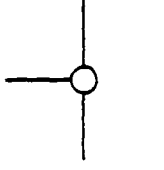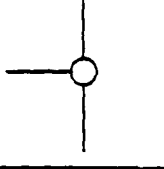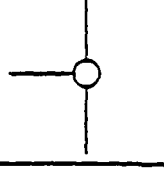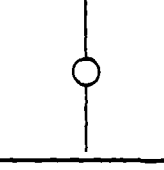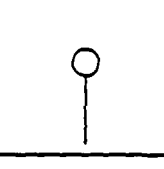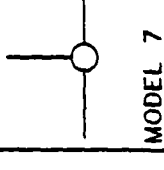
Model 3 was the same as Model 2 except that new wing stiffness measurements became available from other FOG-M structural analyses. With these new section properties, the predicted weak wing axis bending modes dropped slightly, but correlation was neither enhanced nor degraded substantially.

In Model 4, extremely poor correlation was achieved between predicted and measured first fin longitudinal bending mode (378 Hz predicted and 81 Hz measured). The earlier models did not account for the section properties of the short cantilever beam used to support the fins. These beam elements were added and the predicted modal frequency dropped from 378 to 170 Hz but still did not correlate satisfactorily. This significant difference was corrected with the use of an additional static test and will be discussed with Model 7.

Models 5 and 6 were continuations of the effort to study the peculiarities of this particular NASTRAN modal extraction routine. As shown, two wings yield one first wing bending mode, and one wing results in no first wing bending mode. This observation is extremely valuable for future studies. The first mode of any appendage is the most important; consequently, care must be taken in the future when using this subroutine.

Model 7 had two major changes from the previous NASTRAN models. First, the number of nodes used to model the wings and fins was increased significantly in an attempt to improve the correlation of the second and third weak axis wing bending modes and the second weak axis fin bending modes of vibration. The wing nodes were increased from 4 to 20 and the fin nodes increased from 2 to 10. Some improvement was obtained but the frequency correlations did not substantially improve. The mode shapes did correlate extremely well for all these modes.

20

TABLE 18. NASTRAN FEM Sensitivity Analysis.

MODE OF VIBRATION	MODEL 1	MODEL 2 3 WING	MODEL 3 NEW WING STIFFNESS	MODEL 4 FIN SHAFT ADDED	MODEL 5 2 WING	MODEL 6 1 WING	MODEL 7 ADDED WING & FIN NODES & NEW FIN STIFFNESS	MEASURED
1st WING BENDING	20.0 HZ 20.4 20.5	20.2 HZ 20.5	19.0 HZ 19.2	19.0 HZ 19.2	19.3 HZ		19.5 HZ 19.8	19.6 HZ
1st FIN BENDING	43.7 48.6 49.1 49.2	42.6 48.6 49.1 49.2	41.8 48.6 49.1 49.2	40.6 47.1 47.6 47.6	38.6 47.1 47.6 47.7	34.6 47.1 47.6 47.7	48.8 61.7 62.4 62.5	43
2nd WING BENDING	89.7 118.6 118.6 119.5	91.1 118.7 119.2	86.6 112.0 112.2	86.4 111.9 112.2	88.7 112.0	93.5	96.5 120.0 120.6	175 192
1st BODY BENDING	147.1 147.1	146.5 151.2	144.4 149.4	143.8 148.5	143.7 154.6	148.5 154.3	146.3 151.8	130
1st WING LONG. BENDING	167.0 168.4 168.4 173.4	167.9 168.4 172.1	159.1 161.0 162.8	158.2 158.9 161.1	159.0 159.7	159.8	163.0 164.4 167.0	NOT MEAS'D
1st FIN LONG. BENDING	378.0 370.0 397.2 397.8	378.3 379.0 397.2 397.8	378.2 378.7 397.2 397.8	169.7 171.9 172.6 173.0	169.7 171.9 172.7 172.7	169.7 171.5 172.8 173.0	72.2 72.2 72.3 73.0	81
2nd FIN BENDING	233.2 249.9 251.8 251.8	230.6 249.9 251.1 251.5	225.6 249.9 251.4 251.5	221.6 243.7 245.2 245.2	217.4 243.7 245.2 245.2	209.7 243.7 245.2 245.2	366.5 381.6 383.5 383.5	294 328
3rd WING BENDING	278.2 317.3 318.8 318.8	281.0 317.8 319.0	269.4 298.9 300.0	267.6 298.9 300.0	271.4 300.2	279.1	273.0 338.6 340.0	506

The other change in the model was that static tests were conducted to measure the weak and strong fin axis stiffness. The stiffness was translated into section properties, EI terms, and added to the NASTRAN model. Marked improvement was obtained in the fin longitudinal (X- direction) frequency prediction. The predicted frequency dropped from 170 to 72 Hz which compares satisfactorily with the 81 Hz measured. The new weak axis stiffness increased the first bending mode prediction from 41 Hz (Model 4) to 49 Hz (Model 7) compared to 43 Hz measured. The second weak axis fin bending mode prediction was enhanced, i.e., 226 Hz in Model 4, 367 Hz in Model 7, and 294-328 Hz measured. Results of this analysis are summarized in the Lessons Learned Chapter.

VI. LESSONS LEARNED.

A. The length of the stinger connecting the exciter to the test article should be kept as short as possible (Fig. 43). Longer stingers result in relatively low frequency lateral vibrations which induce vibration amplitudes into the article under test.

B. The procedures for using the force transducer recommended by the manufacturer must be carefully followed. Extreme dispersion in test results was found when the tightening torque and mating lubricants were not used as specified. A factor of 2 was found in frequency for the same lower frequency modes of vibration.

C. A control accelerometer should always be used in making the modal measurements in the normal mode or random response approach. Limited instrumentation results in the exciter being turned on and off during the process. Only by recording a reference accelerometer during each step of the process can a baseline be established to give validity to the procedures.

D. A major problem was encountered during the first attempt to measure the first body bending mode of vibration. The data was inconsistent from test setup to test setup. The problem was identified as loose joints which hold the cylindrical body shell members together. There are seven structural joints which connect the various missile subassemblies. Screws were loose and in some cases missing. A concerted effort was made to replace defective hardware and to tighten all joints. The result was consistent data that correlated satisfactorily with the NASTRAN predictions.

E. Random modal testing of structures is more rapid than normal modal testing and possibly more structured. However, a definite loss for the feel of the data can result since a tendency is to analyze each successive resonance and not identify the significance of the modes and interaction of structural parts that produce less significant localized vibrations. A definite problem exists in the random method when a subcomponent is vibrating at a frequency in the same vicinity as the structural mode under investigation. Early in this test, the 90 Hz resonance associated with the cantilevered fiber optics spool and probably with the gimbaled TV seeker was thought to be the first bending mode of the airframe. Random vibration measurements along the body of the missile indicated the 90 Hz to be the first bending mode of the airframe which was a totally erroneous conclusion. Typically, when a subcomponent is vibrating close to a major structural mode, the mode shape will assume the shape closest to the nearest major structural mode. Again, a methodical approach should be followed by starting with the lowest frequency modes, correlating these modes with a mathematical model one at a time, investigating localized resonances, and progressing to the next higher frequency. In addition to this structured approach, it is recommended that a mixture of the normal mode and random response techniques be used to cross check for error in future tests.

F. Great care should be exercised in using some of NASTRAN's modal extraction subroutines. As discussed in the previous paragraph, predictions for the critical first bending modes of appendages such as wings and fins can be lost if such care is not used.

G. All tools available should be used by the analyst/tester to correlate the mathematical models such as static load/deflection tests and retests, and iterations of the mathematical model; and repeat modal testing if required. As discussed in detail in Chapter II, MISSILE AIRFRAME ANALYSIS, careful examination and separate computer runs are sometimes necessary to identify the less flexible body bending modes when masked by the significantly more flexible vibration of wings and fins.

VII. CONCLUSIONS

The first eight modes of vibration of a FOG-M mock-up airframe were measured. One additional mode of vibration was indicated during a previous vibration survey and is included for completeness. These nine modes of vibration and the predicted NASTRAN structural modes are summarized in Table 19. The first bending modes of the primary missile components (wings, fins, and missile body) were successfully correlated as to frequency and mode shapes and the correlation was excellent for some modes, i.e., first wing bending.

The higher bending mode shapes correlated well all the way through the third bending mode of the wing. The modal frequencies for the higher modes of vibration did not correlate. Possible sources for this lack of agreement were offered so that future mathematical models can be improved. Further iterations of the mathematical model could have been pursued until more successful higher mode frequency correlations were obtained, but this process was not followed for the following reasons:

- These tests were primarily intended to demonstrate the versatility and power of modal analysis and testing. This goal was achieved.

- The structure under study was not a flight version of the FOG-M

- The first bending modes of vibration that were correlated are by far the most important and represent those modes of vibration where the maximum deflection and hence the strain and stress energy are concentrated.

The stated objectives of this program were met and the validity of the NASTRAN model was established. A systematic method was established that, if followed in the future, will ensure that modal tests identify critical modes of vibrations and establish the accuracy of NASTRAN mathematical models.

TABLE 19. Summary FOG-M Mock-Up Modal Test/Analysis.

No.	Mode Description	Normal Mode Frequency	Random Response Frequency	NASTRAN Predicted Frequency	Comment
1	1st Wing Bending Y-Z Direction	20 HZ	21 HZ	20 HZ / 20	Excellent Mode Shape Correlation Figure 18 & 31
2	1st Fin Bending Y-Z Direction	43	46	49 / 62 / 62 / 63	Excellent Mode Shape Correlation Figure 45 & 50
3	1st Fin Longitudinal Bending X- Direction	81	82	72 / 72 / 72 / 73	Excellent Mode Shape Correlation Figure 55 & 57
4	Gimbaled Seeker X- Direction	90	Not Measured	Not Modeled	Reference 1
5	Fiber Spool Y-Z Direction	90	Not Measured	Not Modeled	Shape Not Measured
6	2nd Wing Bending Y-Z Direction	175 / 192		97 / 120 / 120	Mode Shape Correlated Figure 20, 21, 32, & 33
7	1st Body Bending Y-Z Direction	130	Not Measured	146 / 152	Excellent Mode Shape Correlation Figure 12
8	2nd Fin Bending Y-Z Direction	294 / 328	306 / 326	367 / 382 / 384 / 384	Mode Shape Correlated Figure 47, 51, & 52
9	3rd Wing Bending Y-Z Direction	273 / 339	Not Measured	506	Mode Shape Correlated Figure 23

26

VIII. RECOMMENDATIONS.

A. Repeat this process for an IOE FOG-M.

B. Model, measure, and correlate the gimbaled seeker first mode of vibration for the gimbaled seeker.

C. Model, measure, and correlate the fiber spool first mode of vibration for the fiber spool.

D. Apply pneumatic pressure tc the fin actuating systems, remove any remaining large nonlinearity, and conduct the fin(s) modal tests with the fins mounted on the missile.

E. Measure and correlate the first longitudinal bending mode of the wing(s).

F. Measure the torsional modes of vibration of the wing(s) and fin(s).

PLAN VIEW
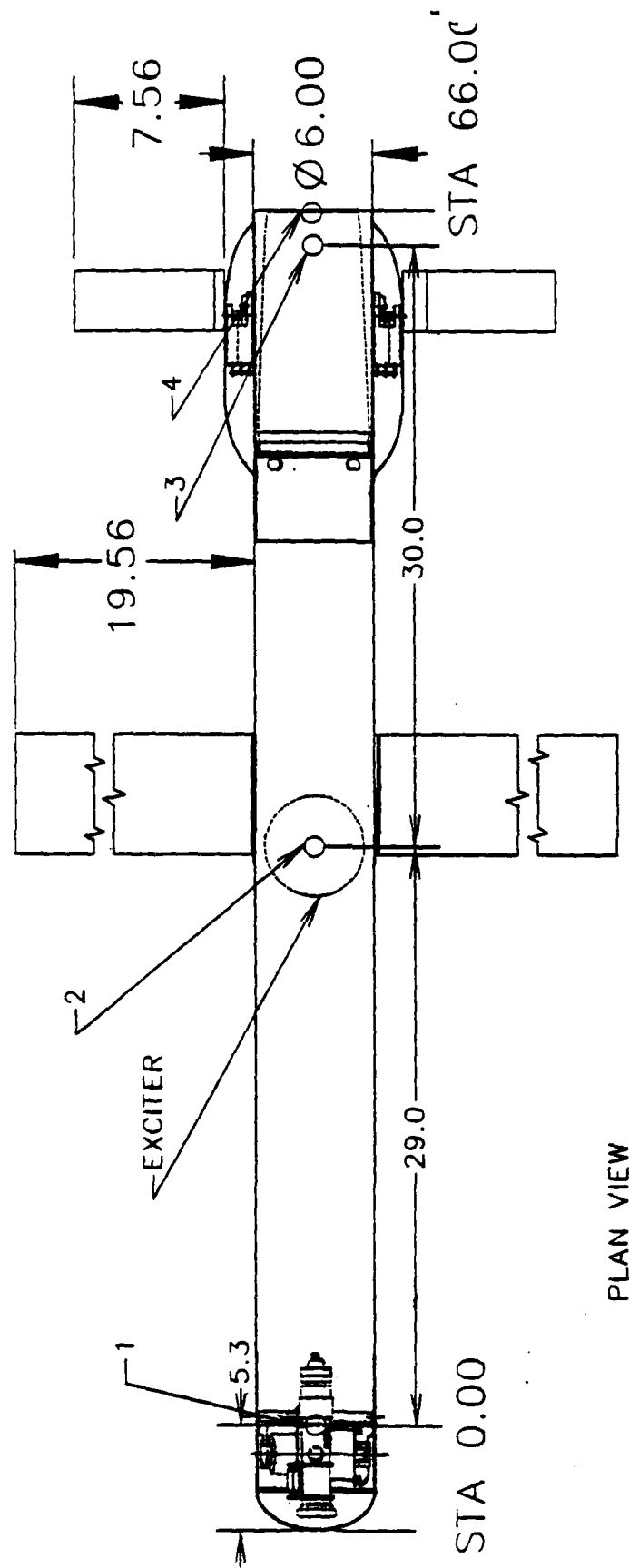
Figure 3. Transducer locations missile body sine sweep.

STA 0.00

STA 66.00

Ø6.00

7.56

19.56

30.0

29.0

5.3

EXCITER

1

2

3

4

23

Figure 4. Sine sweep, transducer 1 & 2.

29

Figure 5.   Repeat of first sine sweep.

30

Figure 6. Sine sweep accelerometers 2 & 3.

31

X=287.81 Hz
Ya=428.583mG·S
POWER SPEC1   F=379.9625   Y=252.6μ
1.0

Mag

Peak
G·S

0.0

15 Hz

FOGM RSP-SPOOL

Yb=184.93mG·S
POWER SPEC2   F=379.9625   Y=387.6μ
3.2

Mag

Peak
G·S

0.0

15 Hz

FOGM RSP-SPOOL
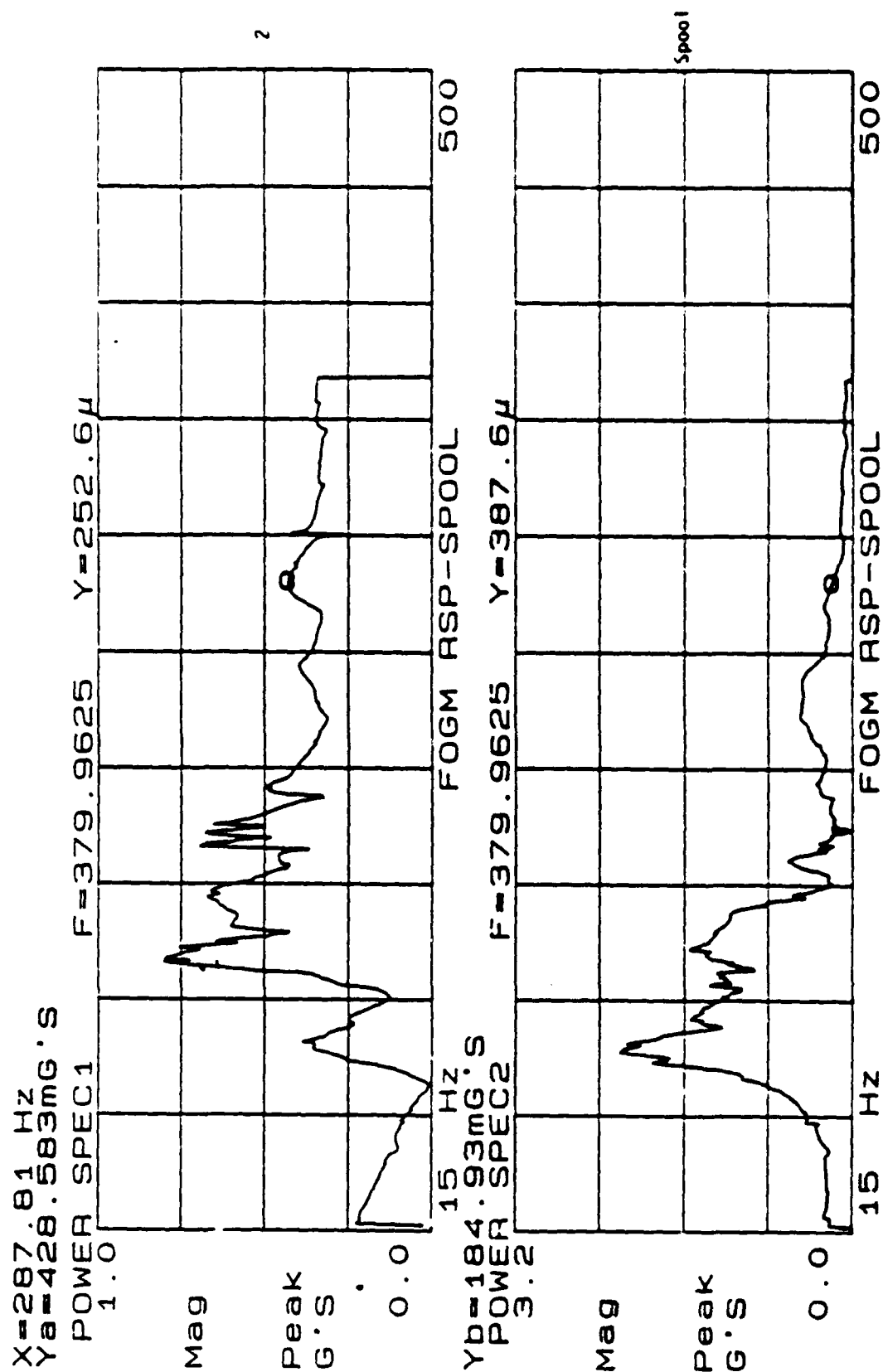
Figure 1. Sine sweep accelerometer 2 & spool.

32
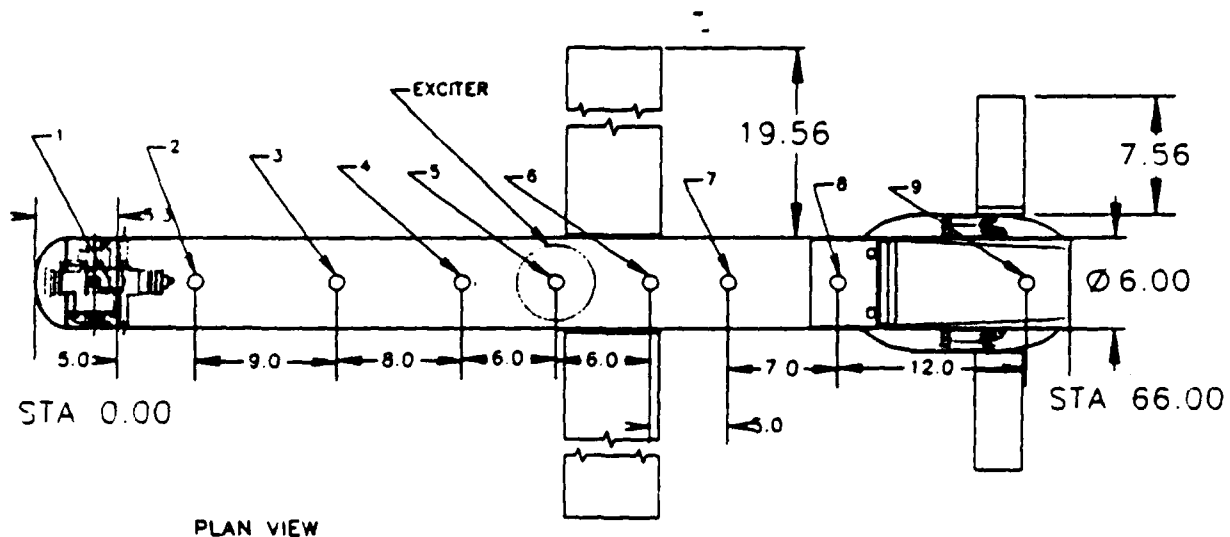
Figure 8. Transducer locations sine dwell tests.
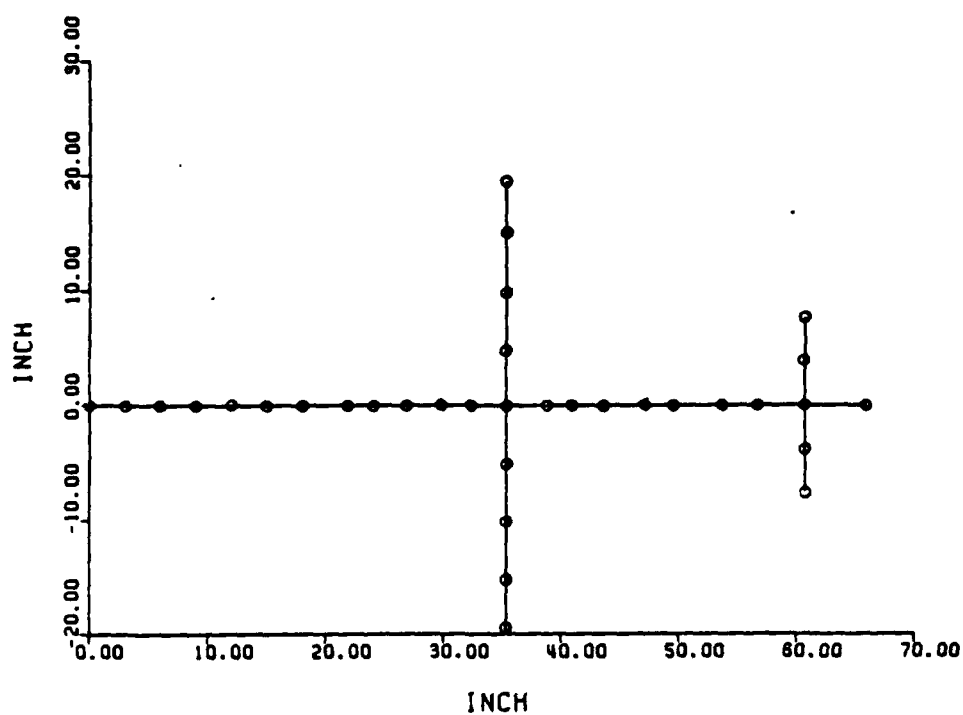
Figure 9. NASTRAN beam model.

33

MAX-DEF. = 1.00000000
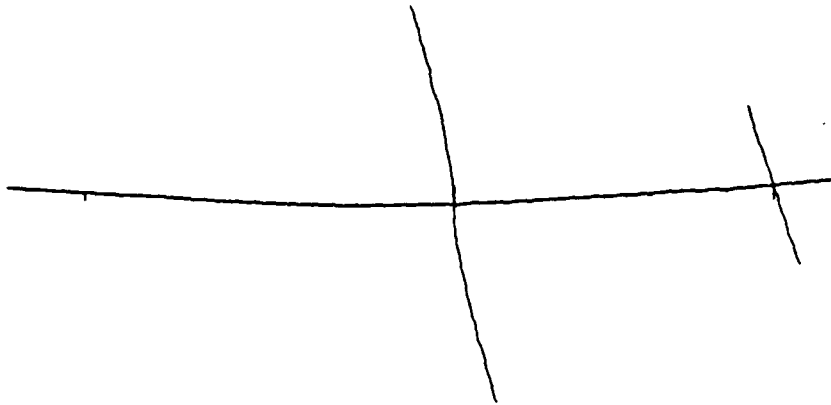
Figure 10. Mock-up missile modal analysis, frequency=145.4 Hz.

1ST BOOT BENDING X-Z PLANE
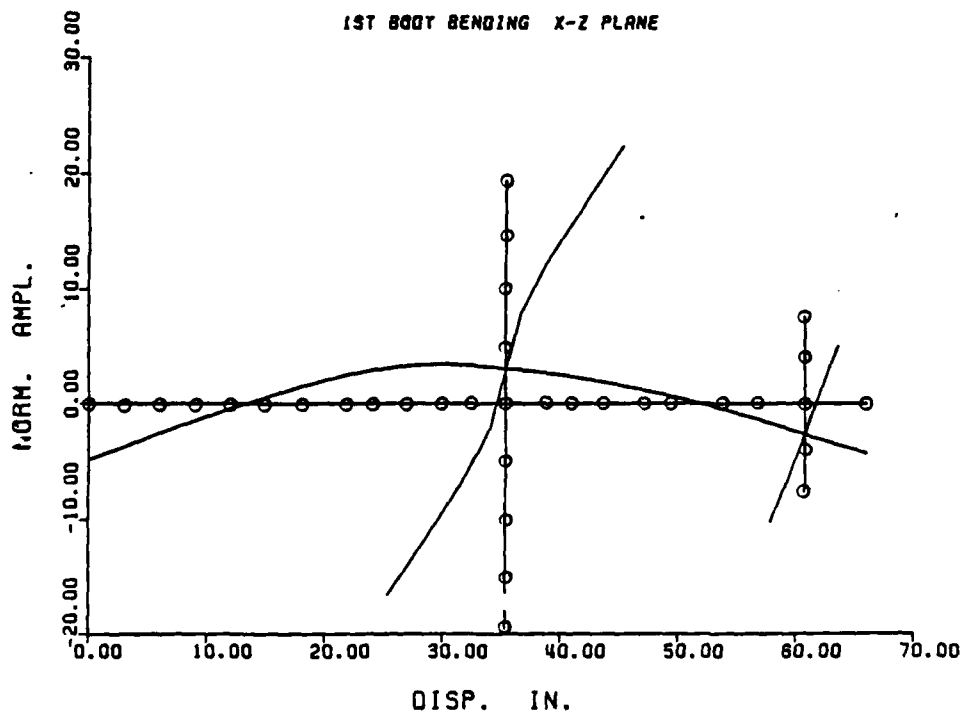
Figure 11. Freq. NASTRAN = 160.83 Hz w/o wings
            freq. NASTRAN = 147.12 Hz distributed mass.

34
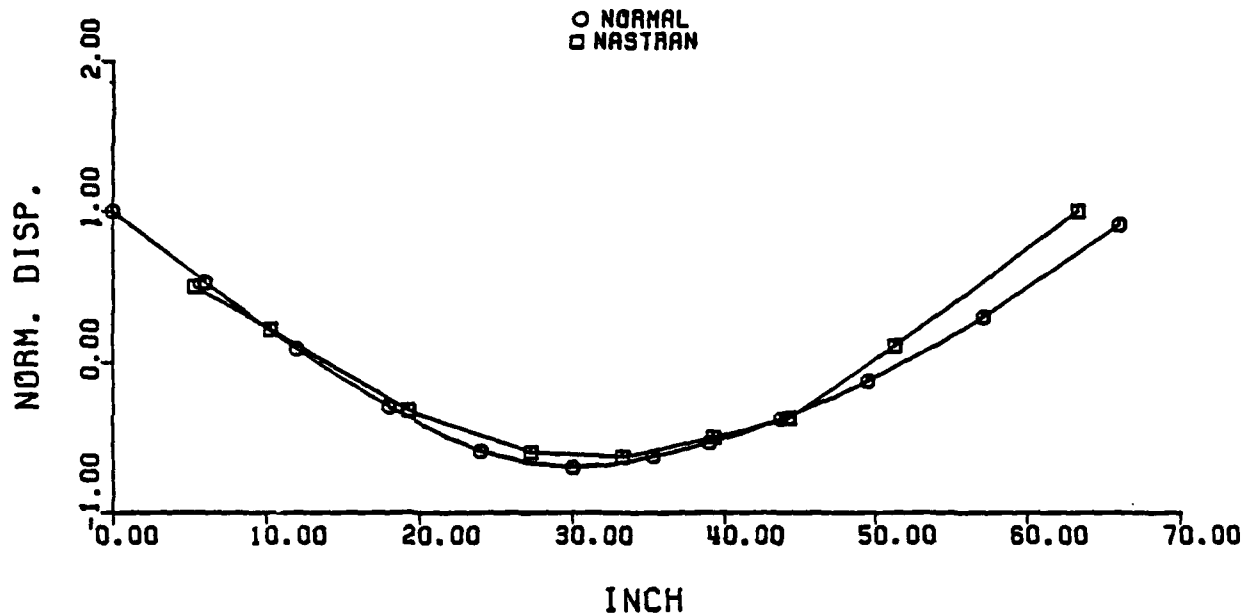
Figure 12. First bending normal mode F = 130.3 Hz
first bending NASTRAN F = 147.1 Hz.
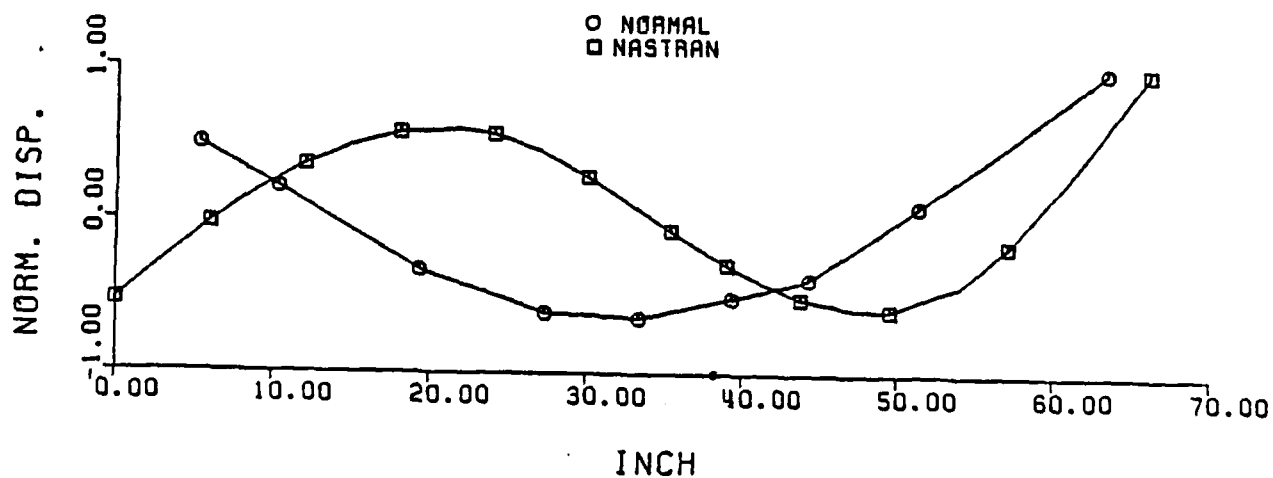
Figure 13. Second bending normal mode F = 267.0 Hz
second bending NASTRAN F = 467.8 Hz.
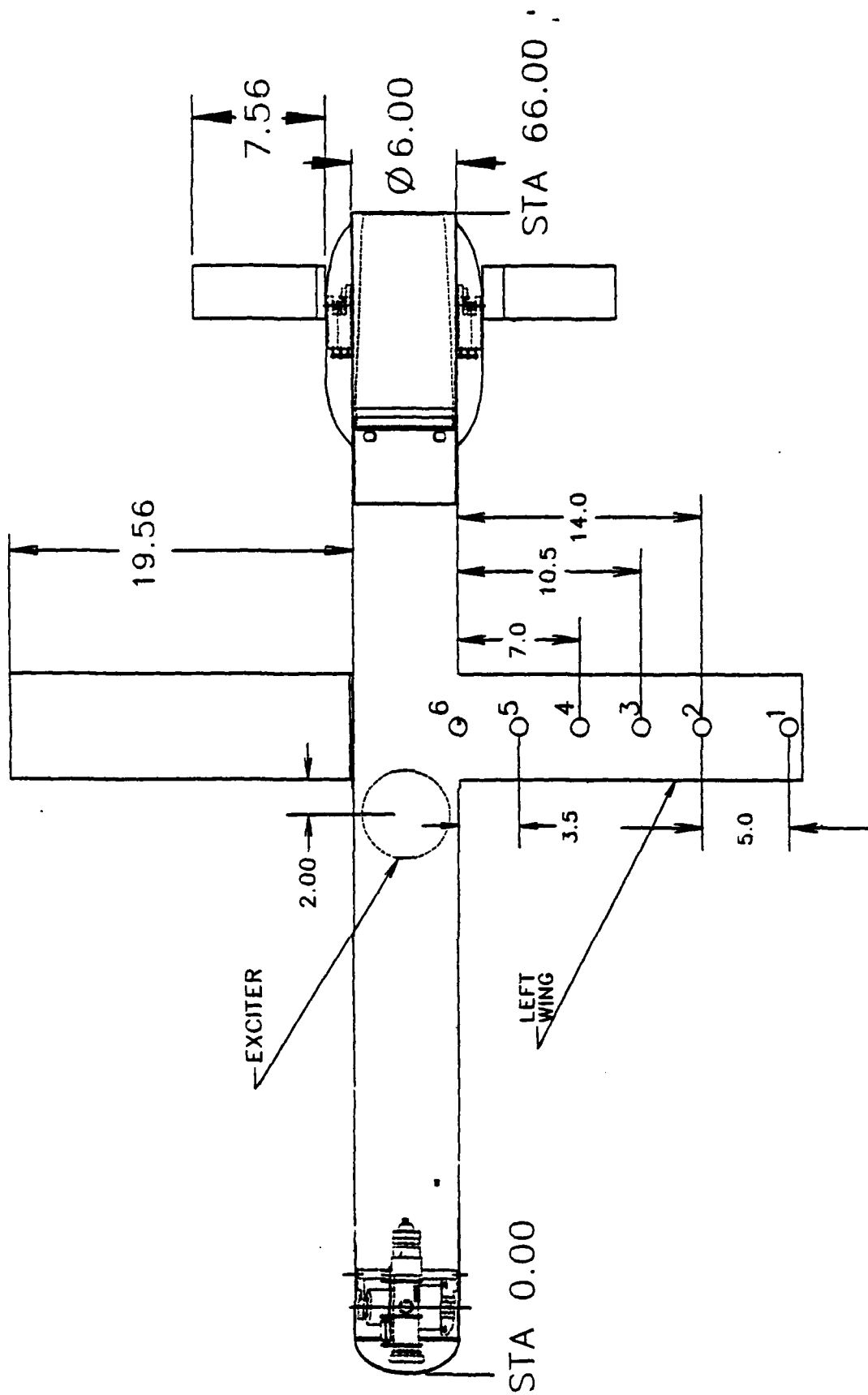
Figure 14. Transducer locations for left wing test.

36

Figure 15. Sine sweep left wing 15-200 Hz.
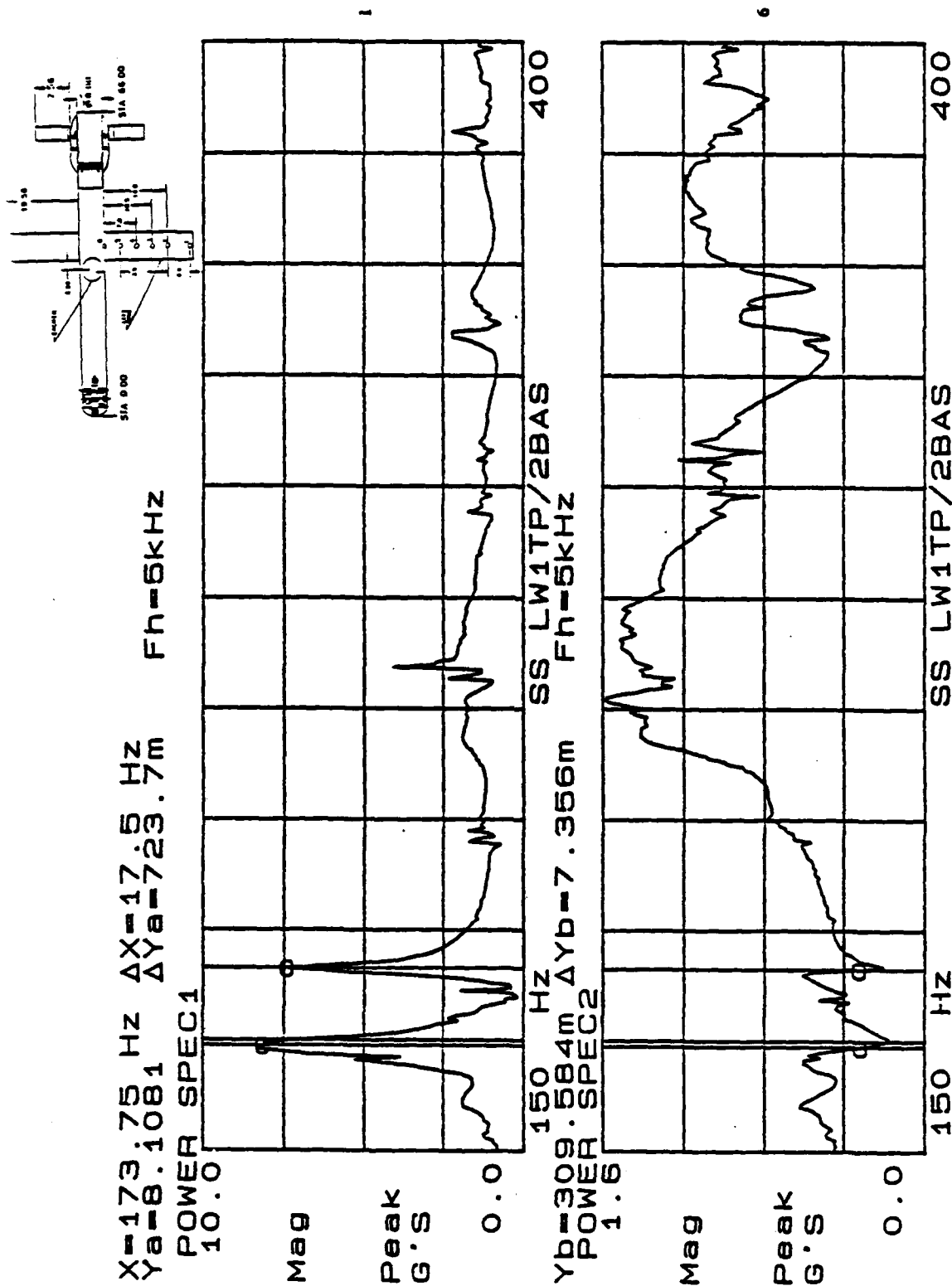
Figure 16. Sine sweep left wing 150-400 Hz.
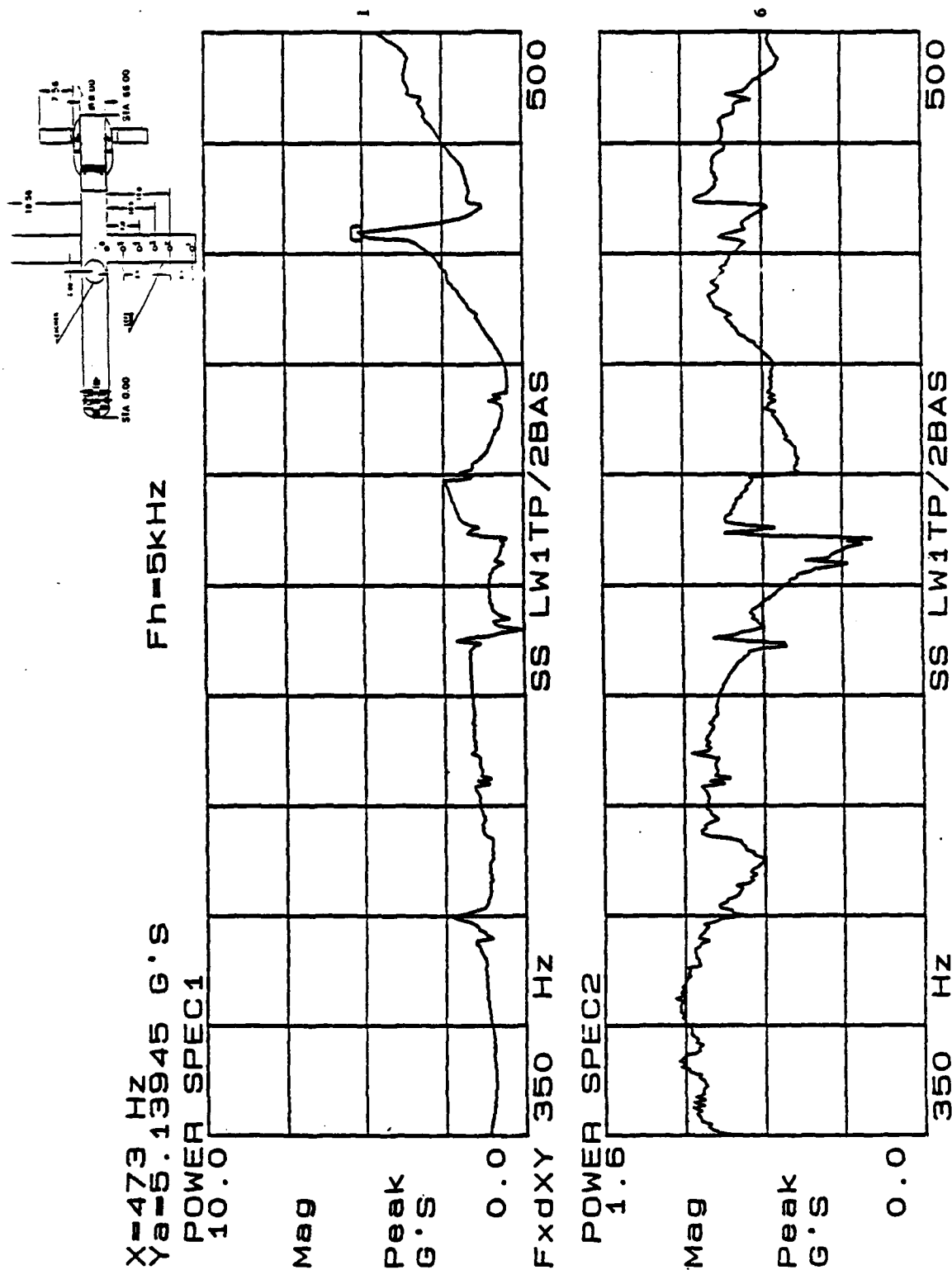
Figure 17. Sine sweep left wing 350-500 Hz.

39
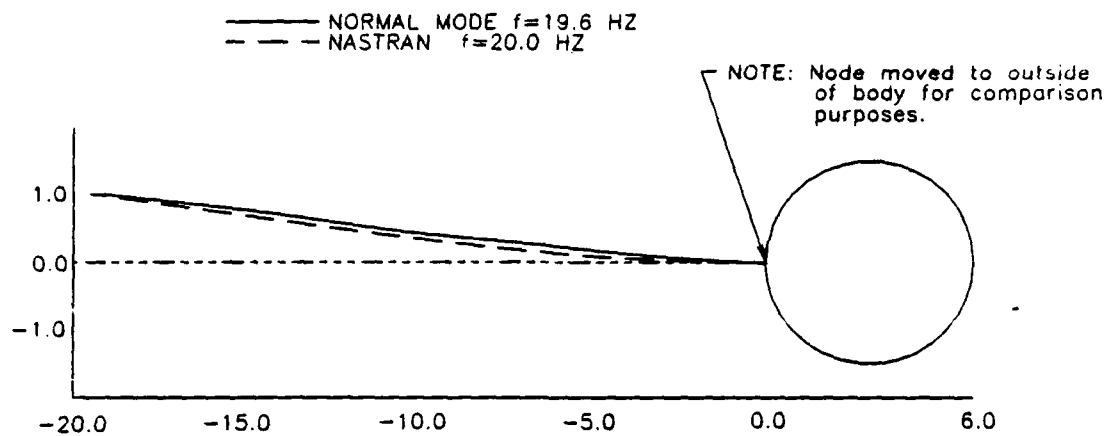
Figure 18. <u>Left wing measured and predicted first bending modes.</u>
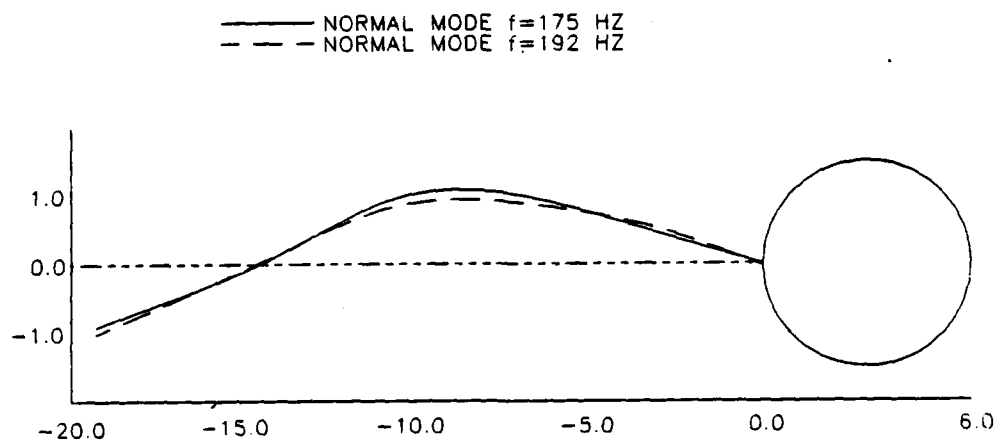
Figure 19. <u>Left wing measured second bending modes.</u>

40
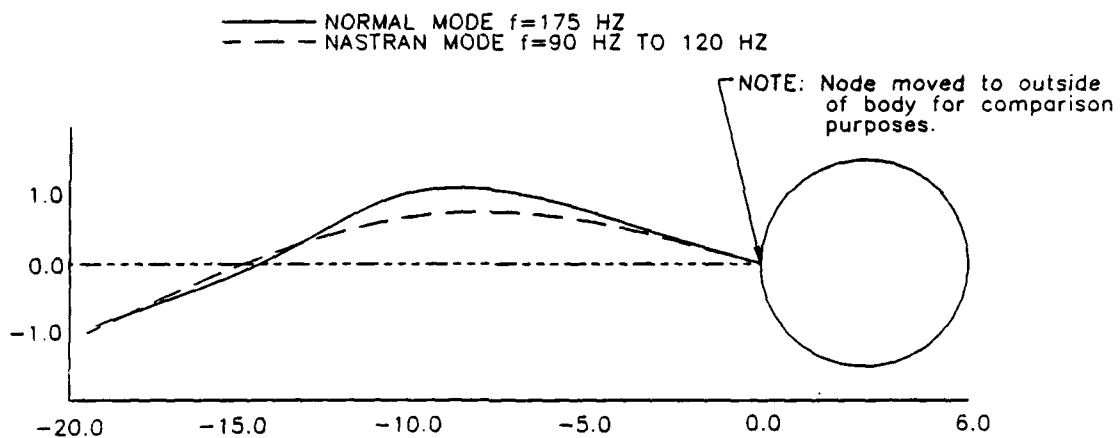
Figure 20. Left wing measured and predicted second bending mode.
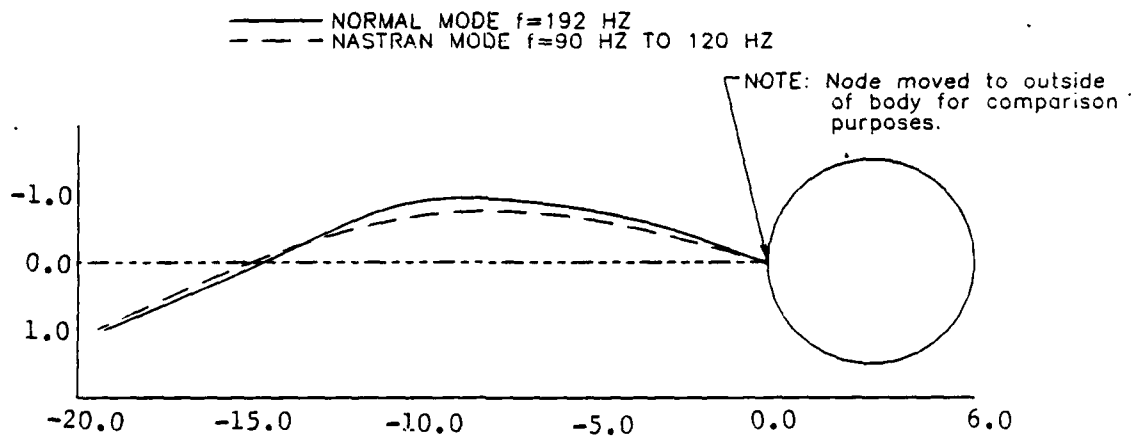
Figure 21. Left wing measured and predicted second bending mode.

41
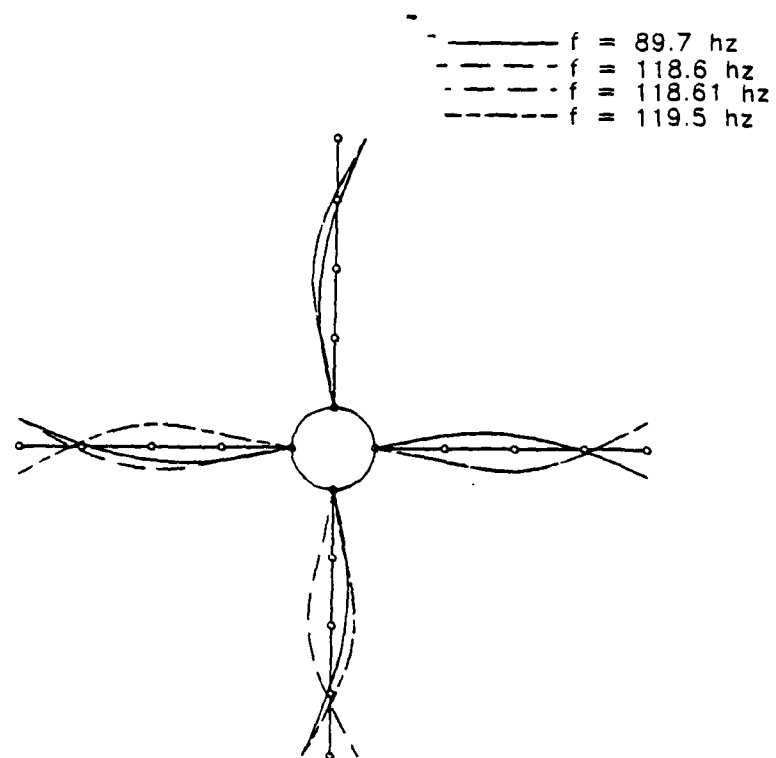
Figure 22. Predicted second bending mode shapes.
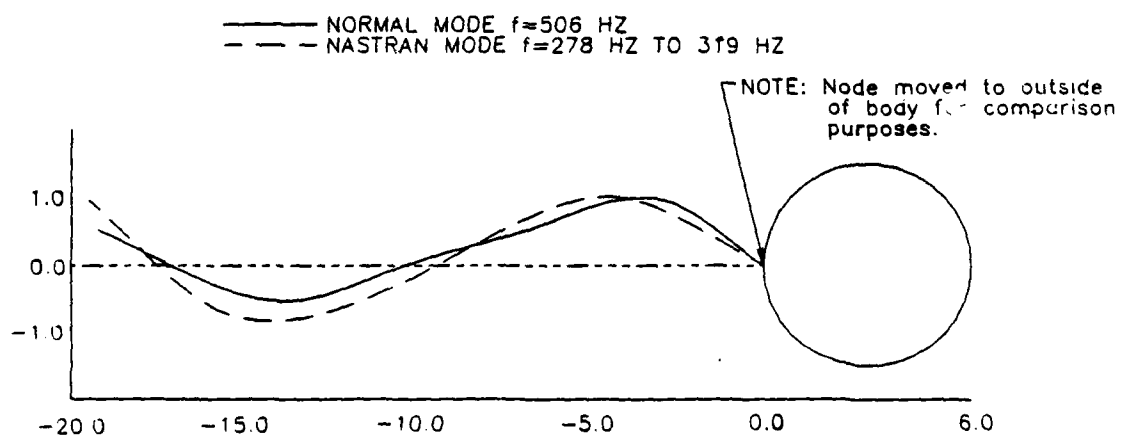
Figure 23. Left wing measured and predicted 3rd bending mode.
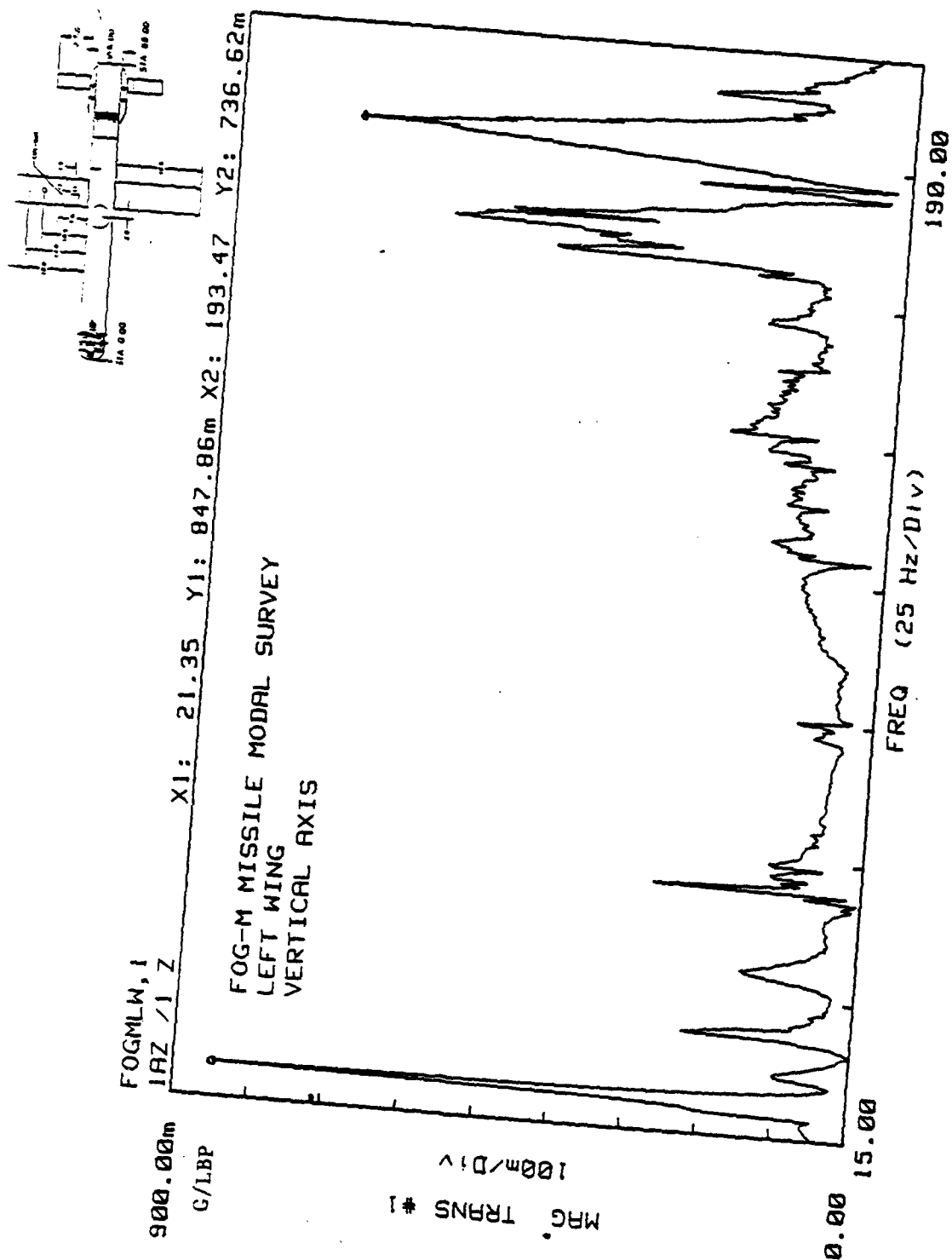
Figure 24. Accelerometer 1, random vibration 15-210 Hz.

43
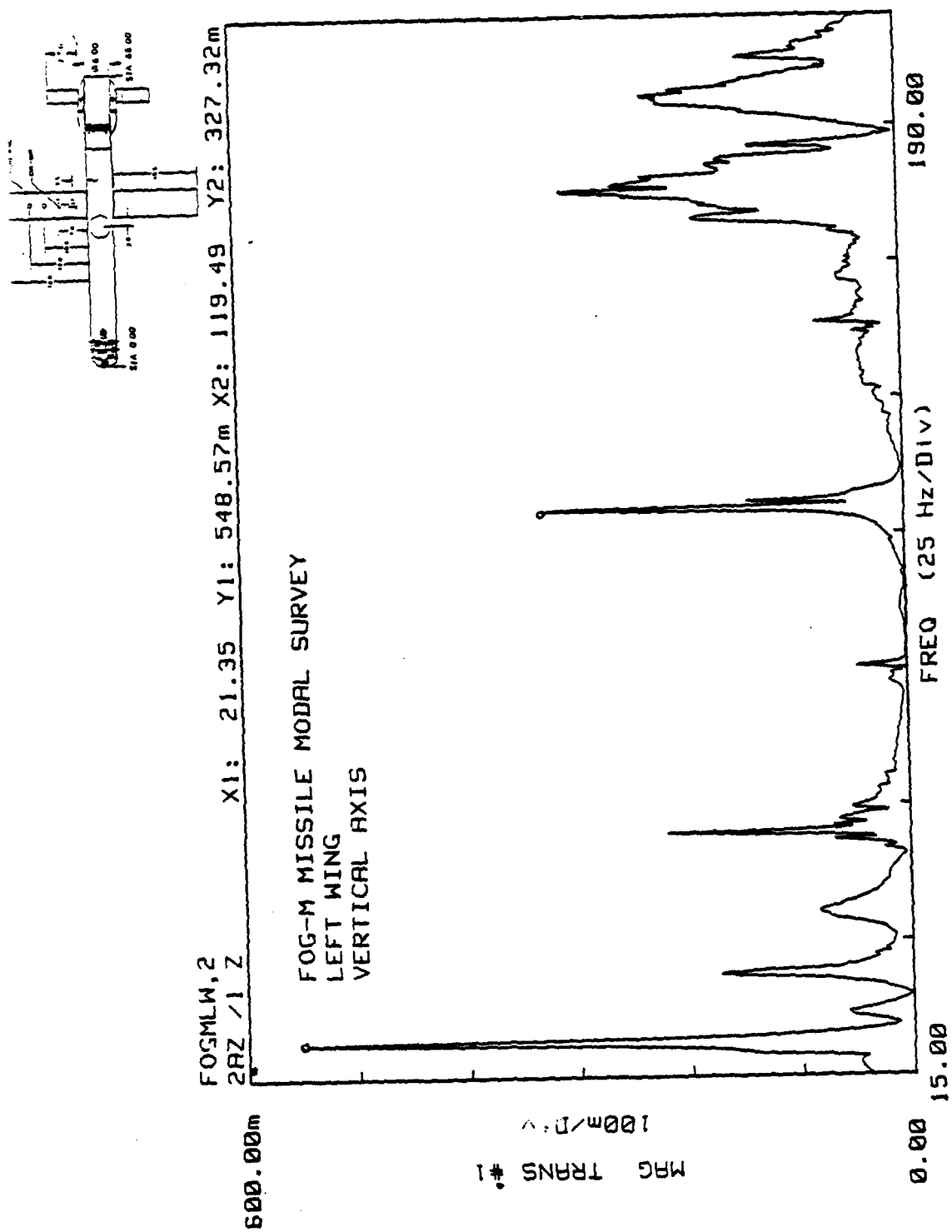
Figure 25. Accelerometer 2, random vibration 15–210 Hz.

44
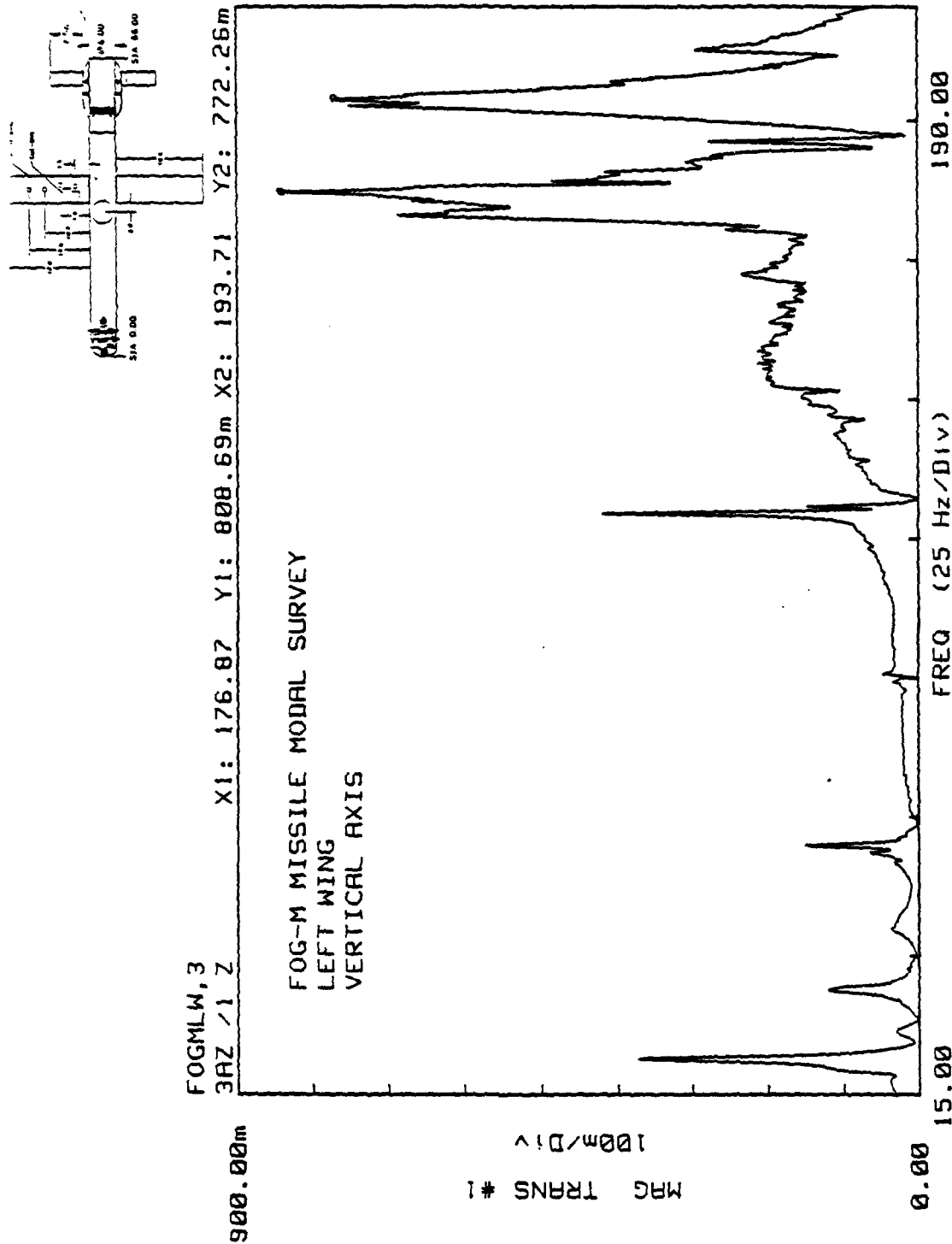
Figure 26. Accelerometer 3, random vibration 15-210 Hz.
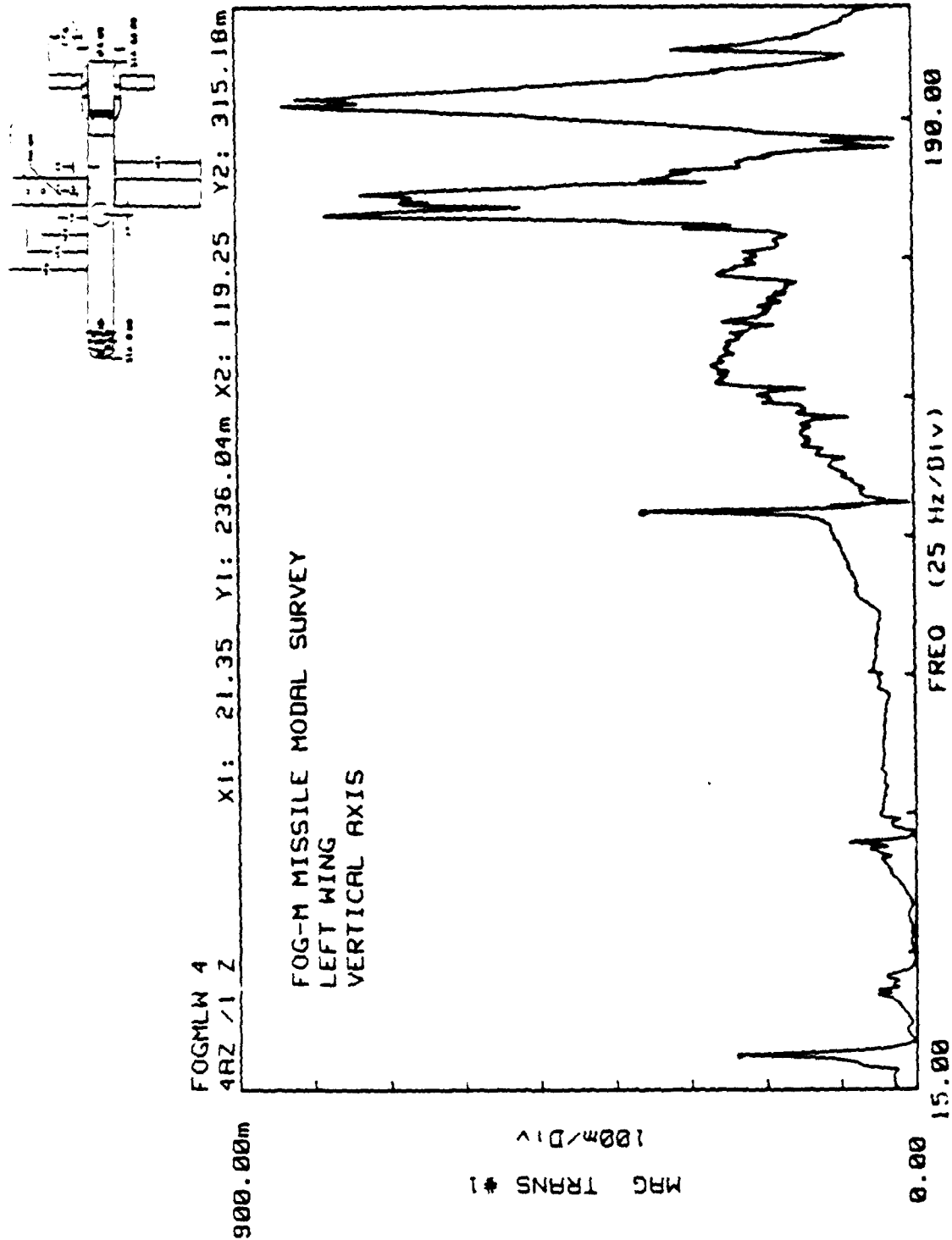
Figure 27. Accelerometer 4, random vibration 15-210 Hz.
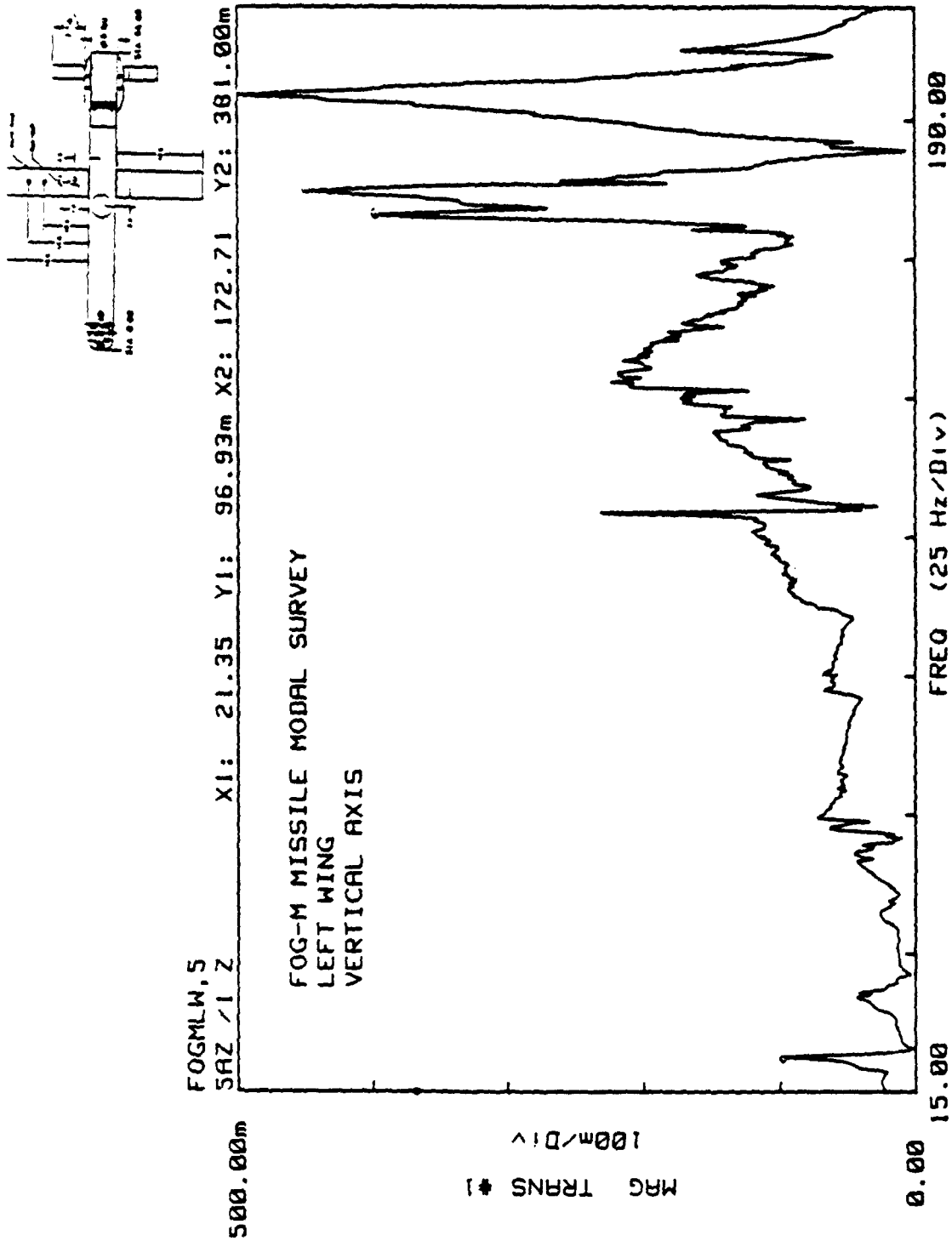
Figure 28. Accelerometer 5, random vibration 15-210 Hz.
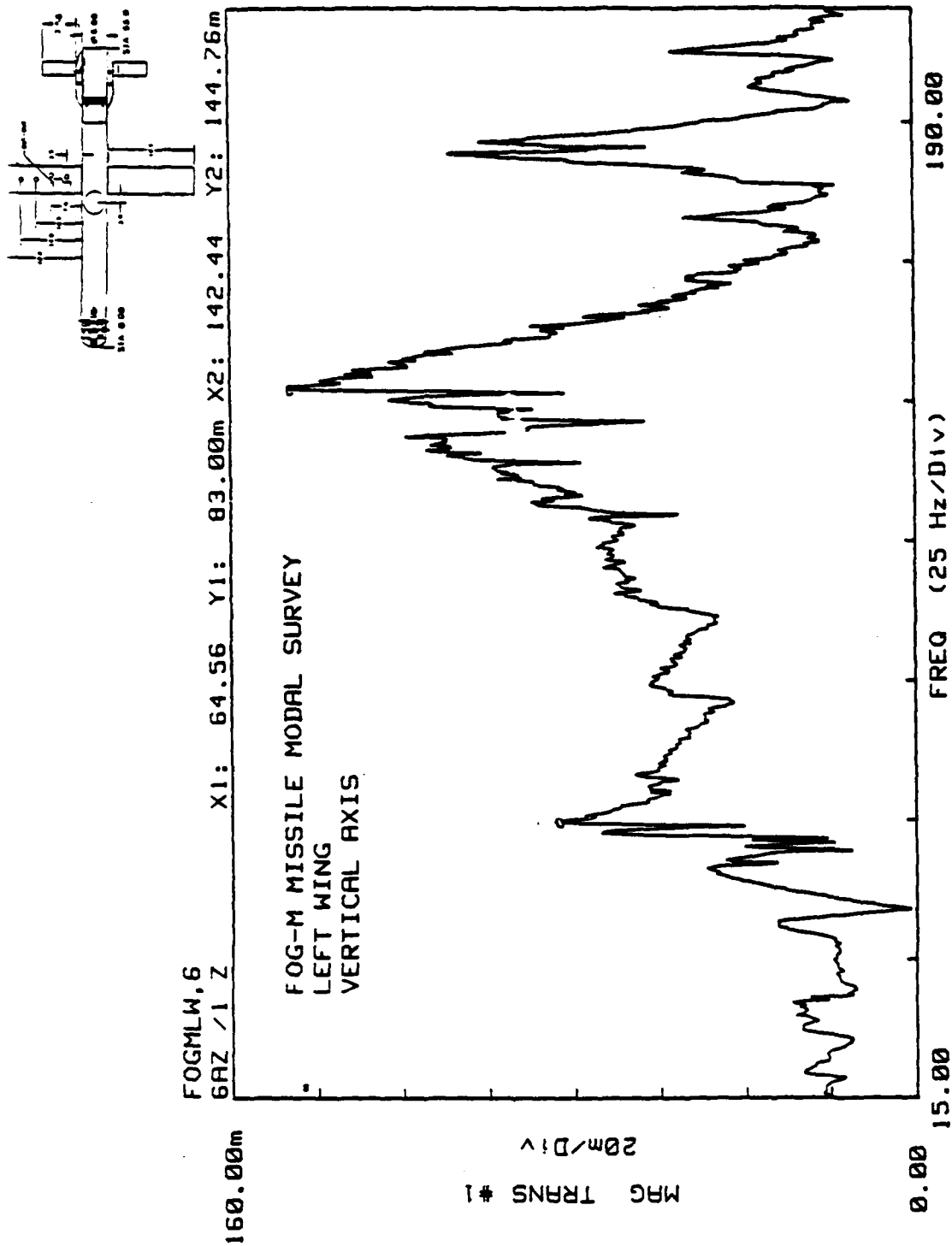
Figure 29. Accelerometer 6, random vibration 15-210 Hz.

Figure 30. Random vibration, left wing "find mode".

Mode # 1	Damp: 1.75 %
Freq: 21.36 Hz	View :<1,0,0>

FOGMLW EXC $Z
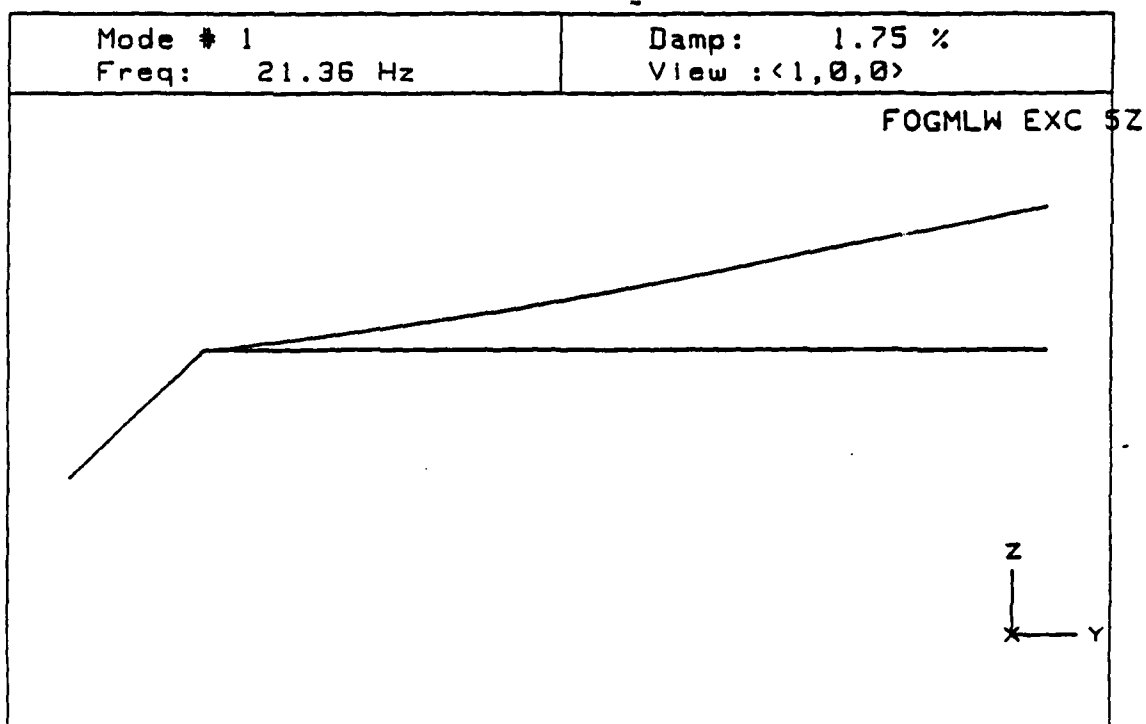
Figure 31. Random vibration mode left wing, first bending mode (21.36 Hz).

Mode # 3	Damp: .54 %
Freq: 172.89 Hz	View :<1,0,0>

FOGMLW EXC $Z
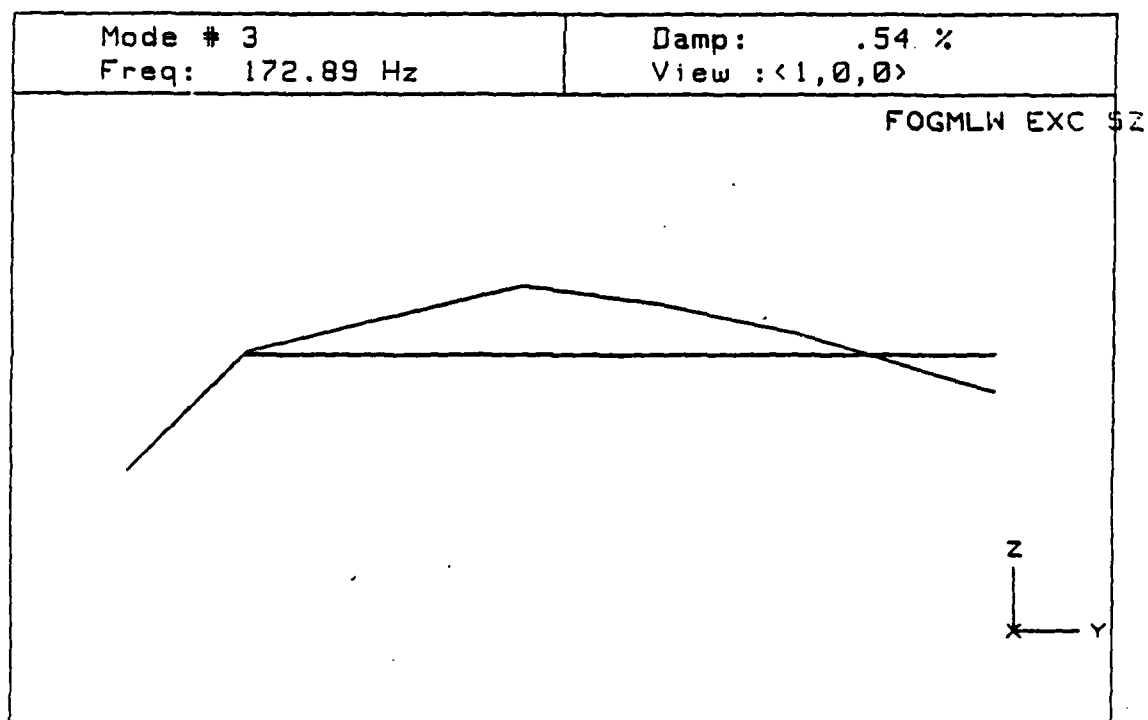
Figure 32. Random vibration mode left wing, second bending mode (172.89 Hz).

Mode # 4   Damp: 1.11 %
Freq: 194.97 Hz View :<1,0,0>

FOGMLW EXC $Z
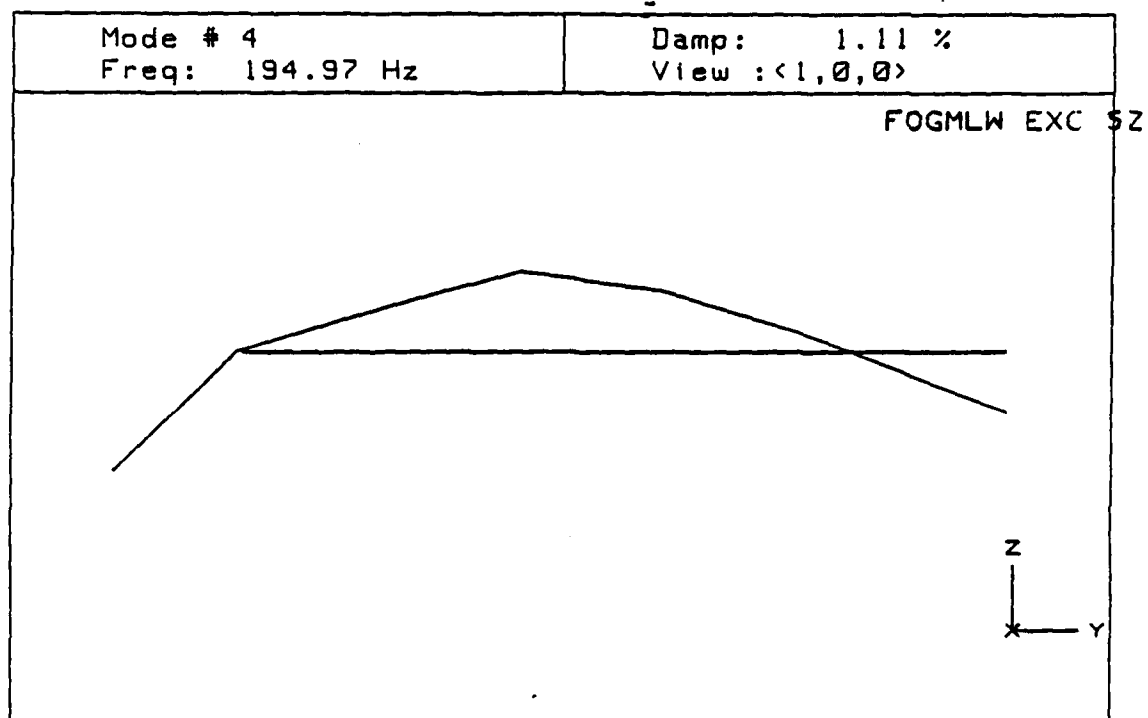
Figure 33. Random vibration mode left wing, second bending mode (194.97 Hz).

Mode # 2   Damp: .19 %
Freq: 119.57 Hz View :<1,0,0>

FOGMLW EXC $Z
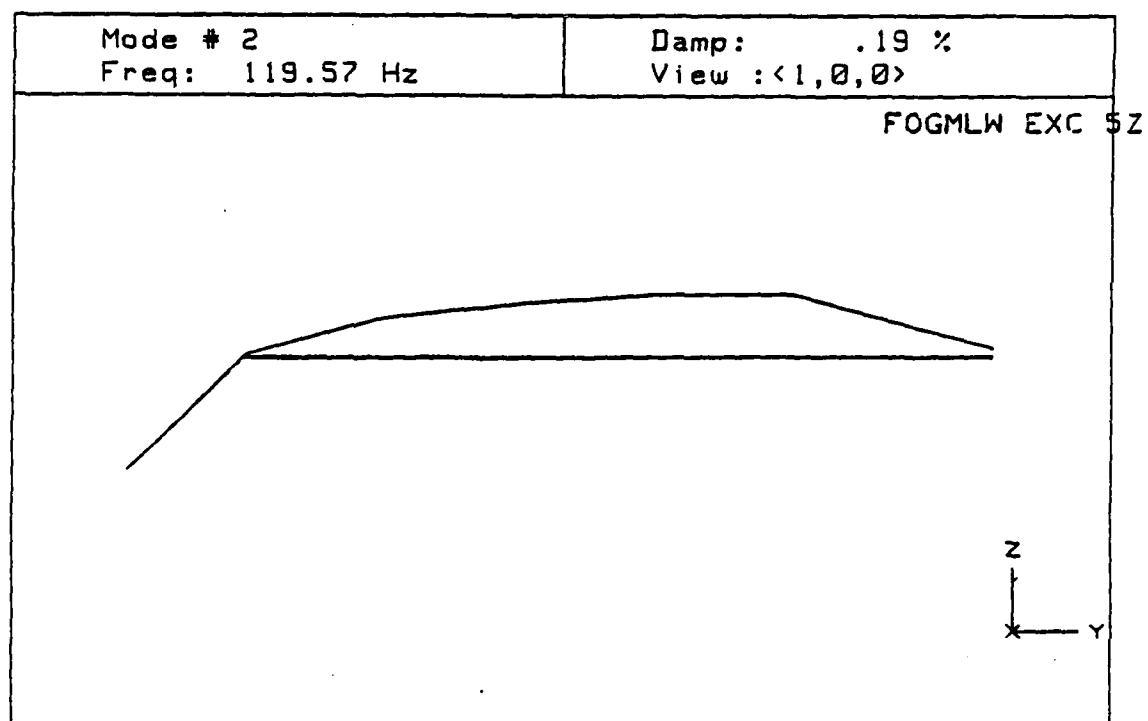
Figure 34. Random vibration mode left wing, (apparent mode equal to 119.57 Hz).
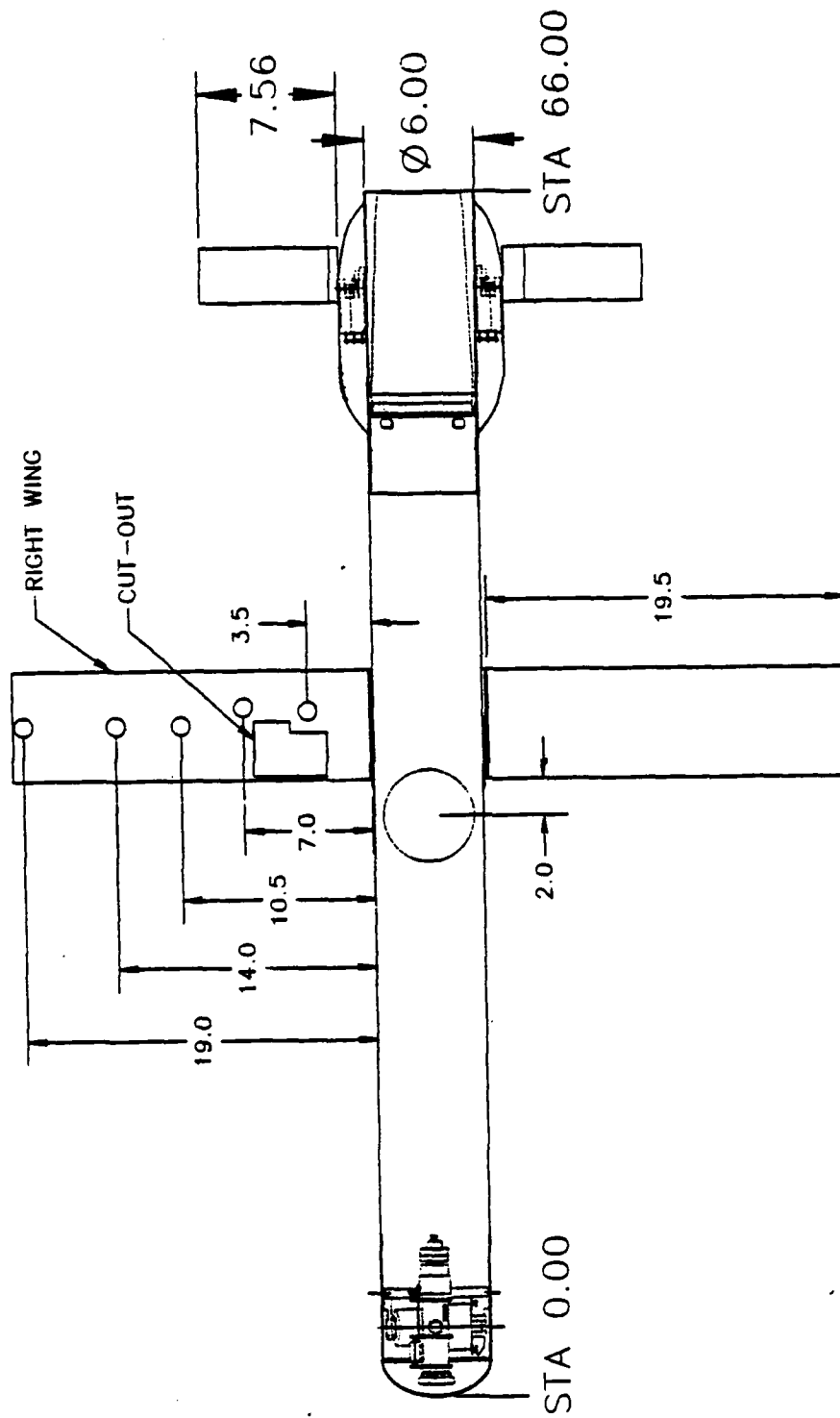
Figure 35.   Transducer location for right wing test.
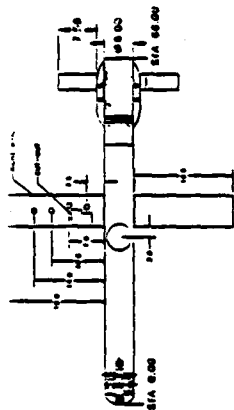
X=20.87 Hz   ΔX=139.6 Hz
Ya=3.16264   ΔYa=6.885
POWER SPEC2
16.0

Mag

Peak
G'S   0.0
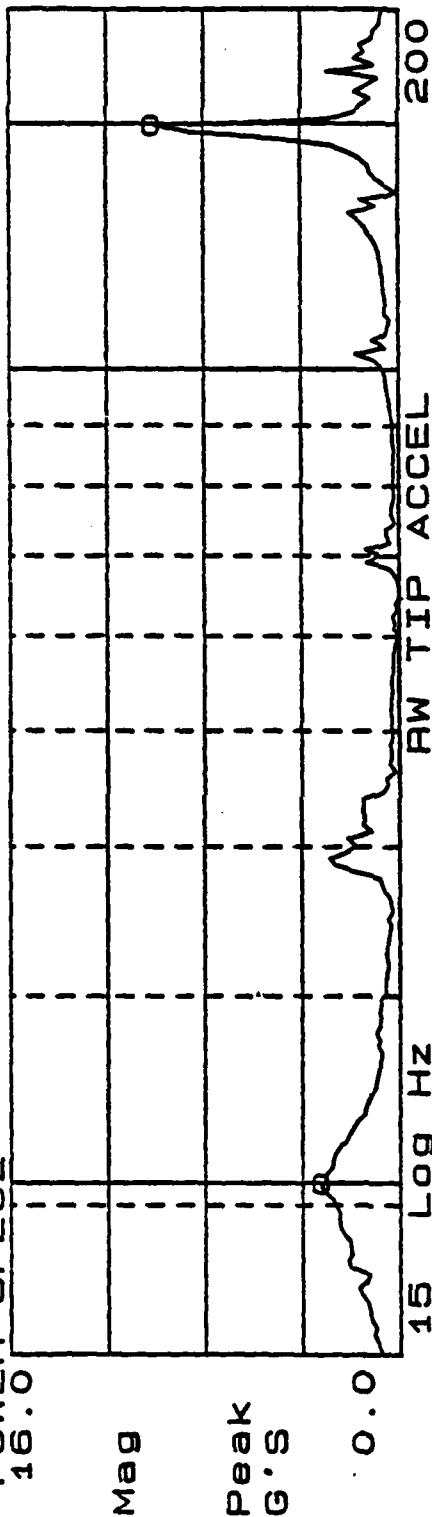
15 Log Hz
Yb=-166.01   ΔYb=504.6 Dg
FREQ RESP
0.0

Phase

Deg

-800

15 Log Hz

RW TIP ACCEL

RW TIP ACCEL
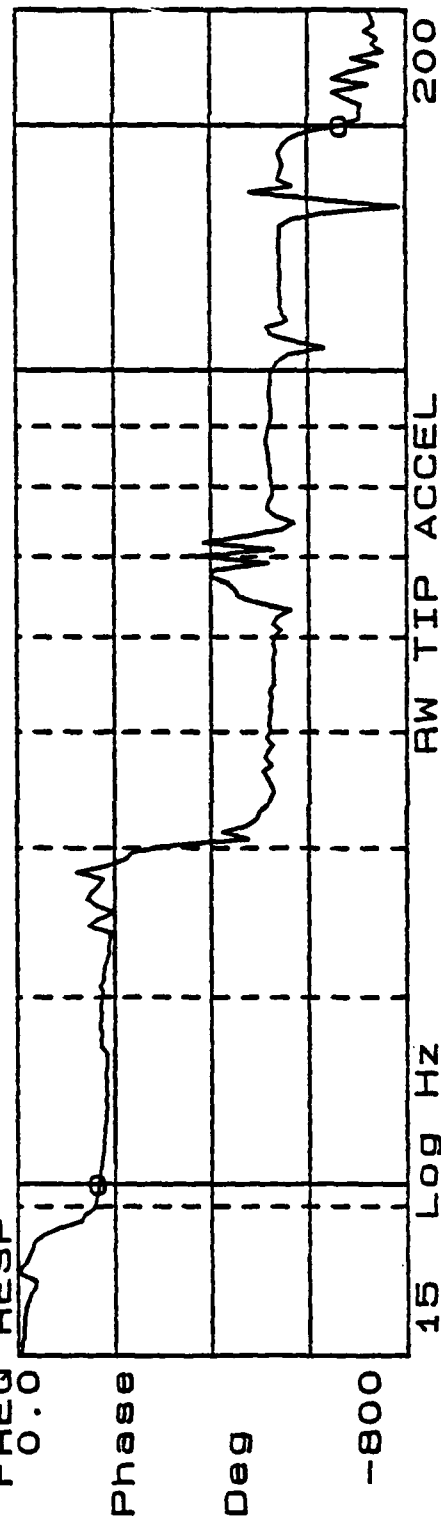
Figure 36. Sine sweep right wing 15 Hz – 200 Hz.

53
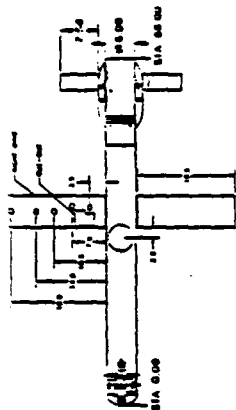
X=214.37 Hz ΔX=55.0 Hz
Ya=4.70022 ΔYa=8.475

POWER SPEC1
16.0

Mag

Peak
G'S
0.0

Yb=681.914m ΔYb=121.4m
150
POWER SPEC2
2.25

Mag

Peak
G'S
250
m

Hz

Hz

1

6

400

400

150

150
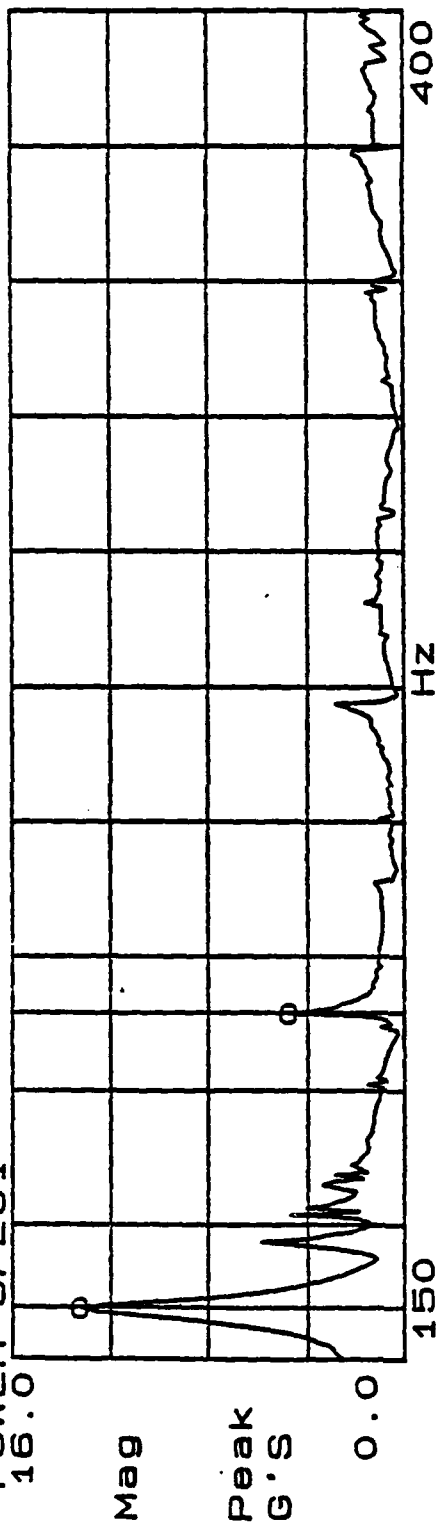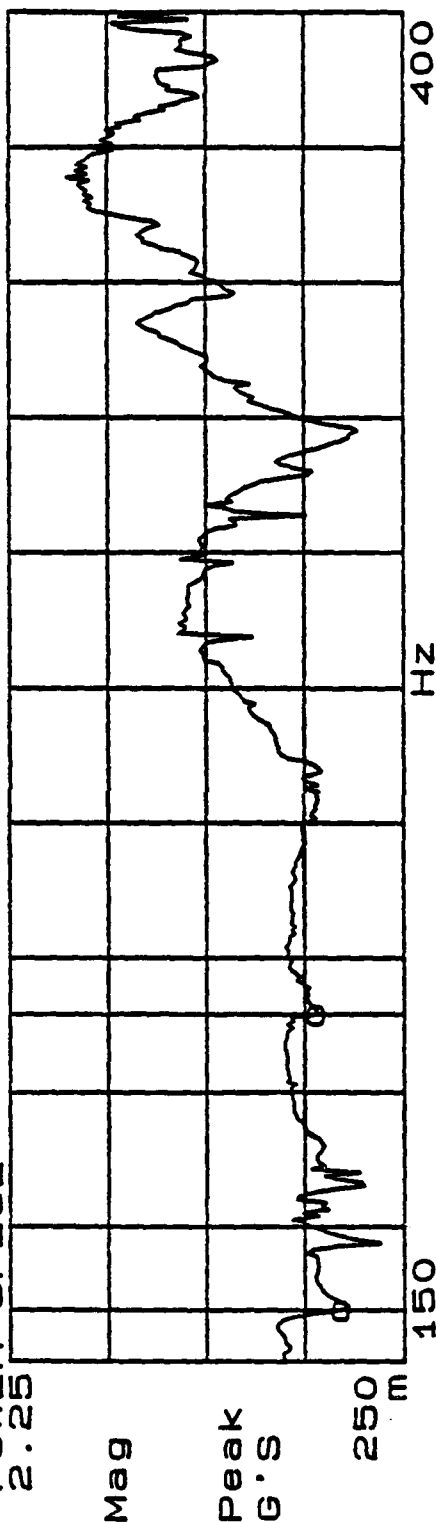
Figure 37. Sine sweep right wing 150 Hz – 400 Hz.

54

Figure 38. Sine sweep right wing 350 Hz - 600 Hz.
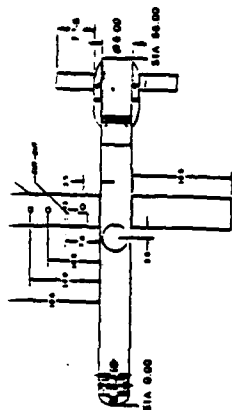
X=432.5 Hz ΔX=48.12 Hz
Ya=5.72357 ΔYa=140.0m

POWER SPEC1
16.0

Mag

Peak
G·S

0.0
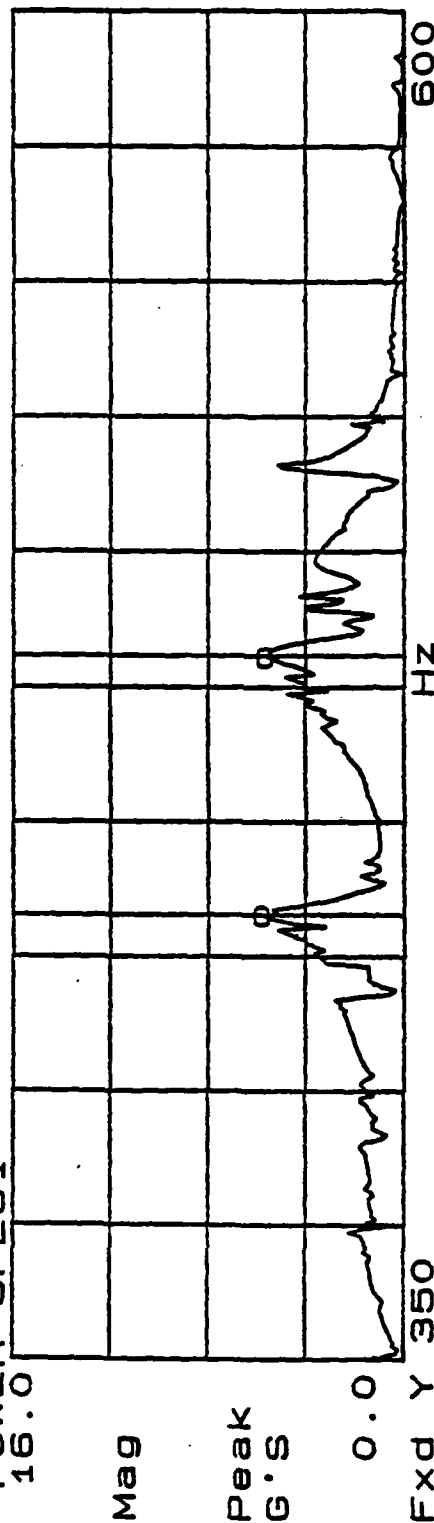
Fxd Y 350   Hz   600
Yb=1.40211 ΔYb=750.2m
POWER SPEC2
2.25

Mag

Peak
G·S

250
m

Fxd Y 350   Hz   SS RW1TP/2BAS   600

55
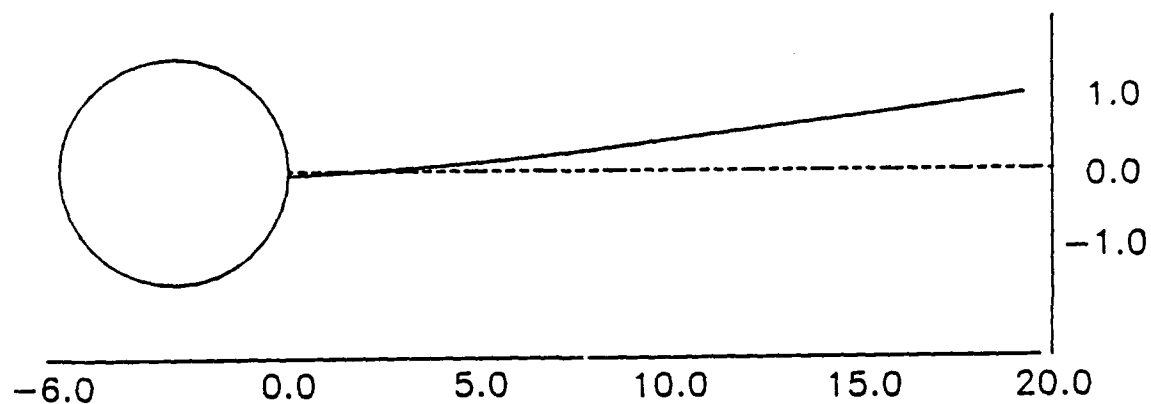
Figure 39.   Right wing first bending mode F = 21.0 Hz.
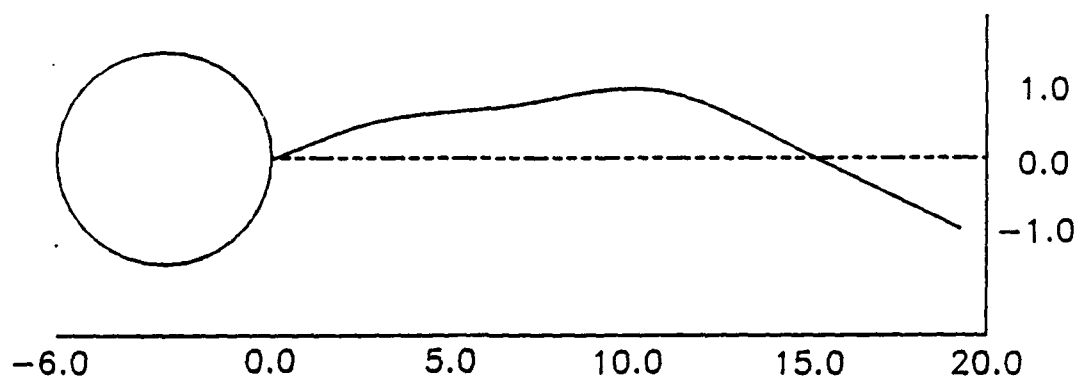
Figure 40.   Right wing second bending mode F = 160.0 Hz.
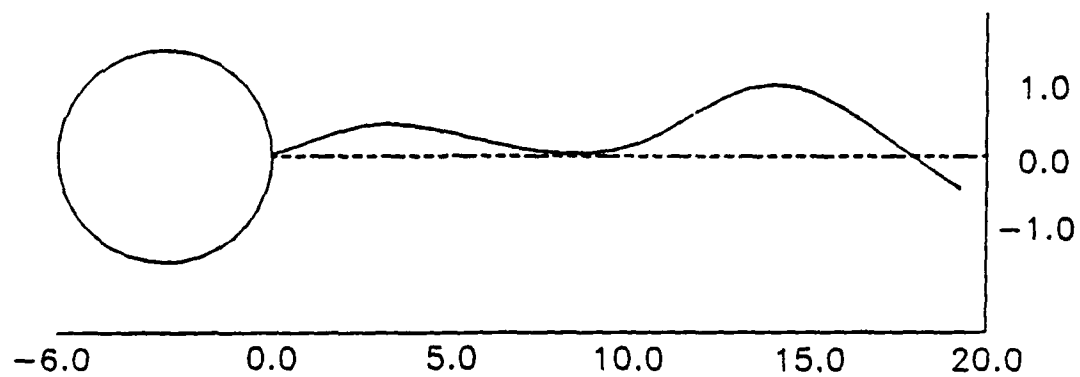
Figure 41.   Right wing bending mode F = 433.0 Hz.
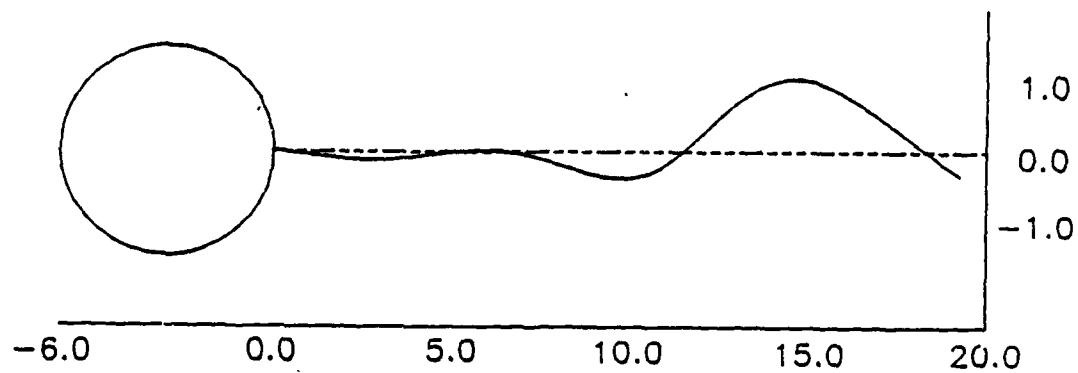
Figure 42.   Right wing bending mode F = 481.0 Hz.
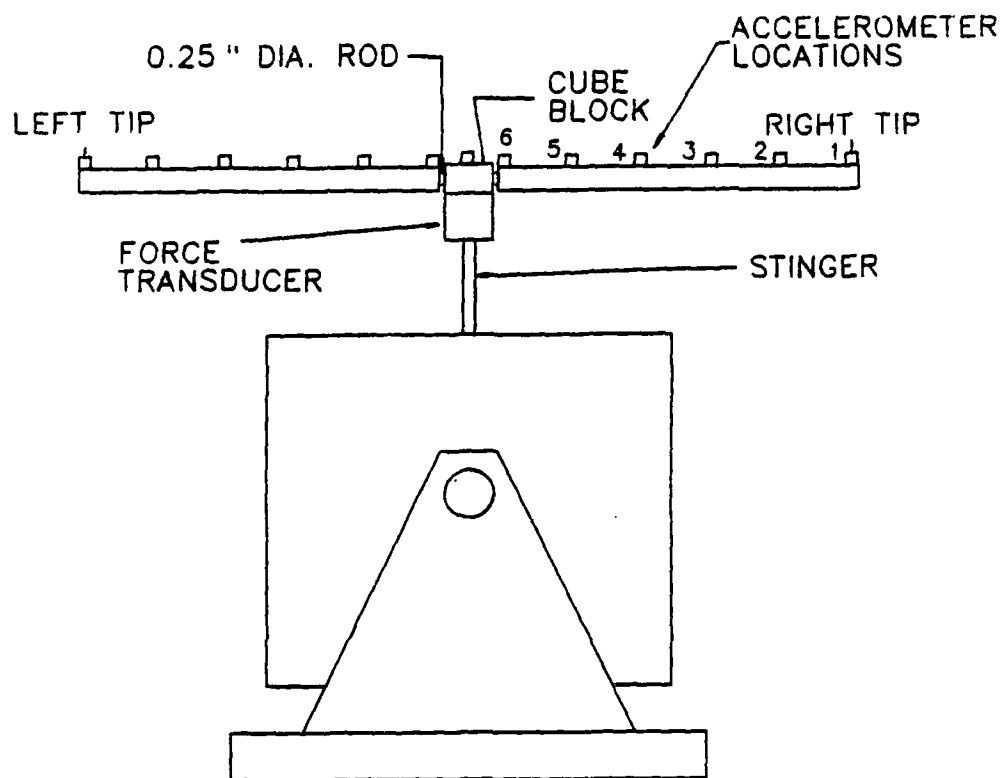
Figure 43.   Fin Y-Z direction test configuration.
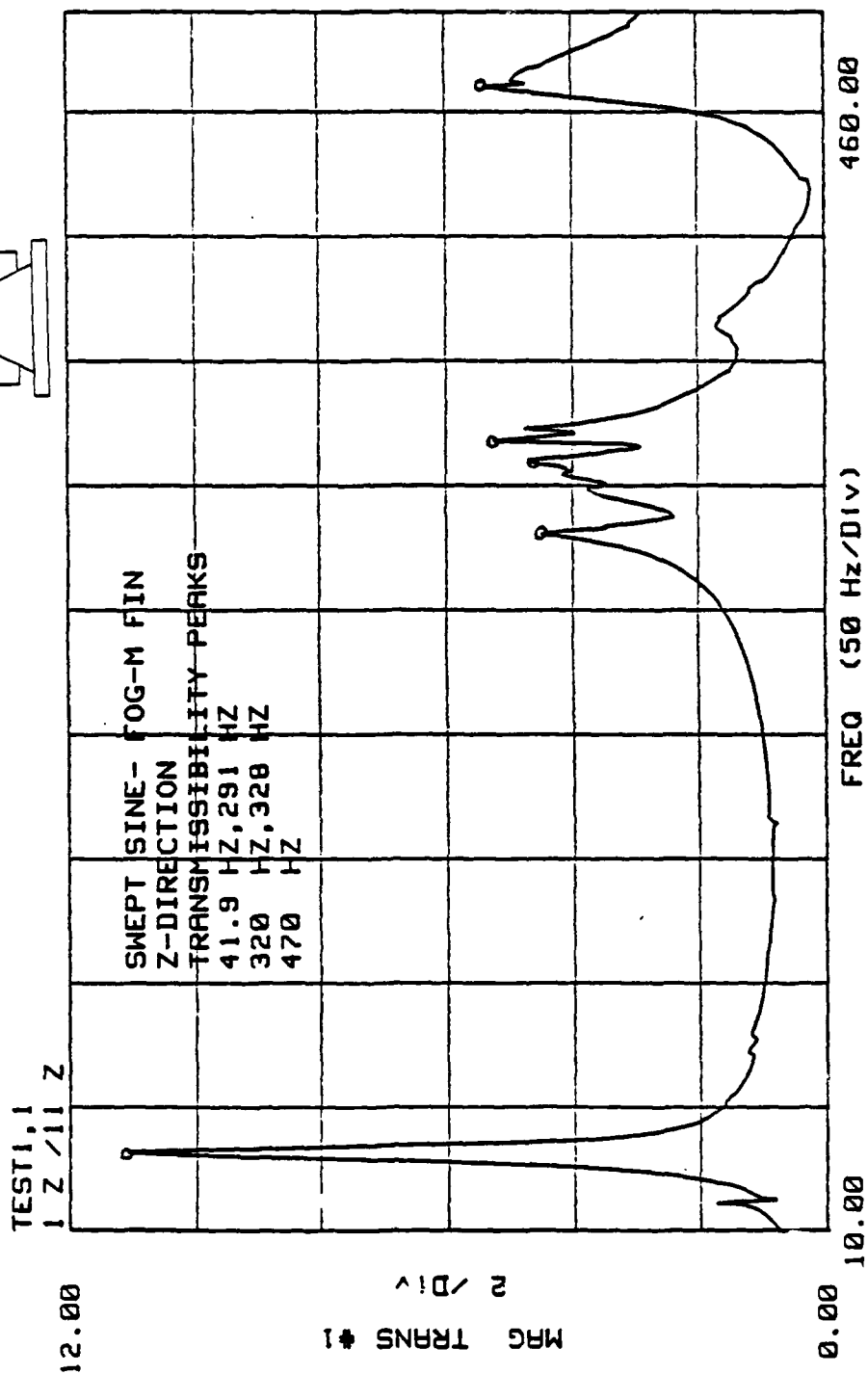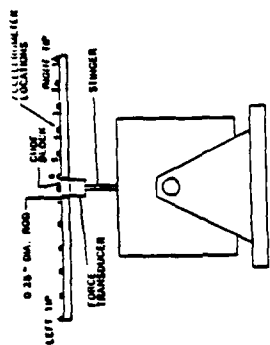
Figure 44. Fins sine sweep frequency range 10-510 Hz.
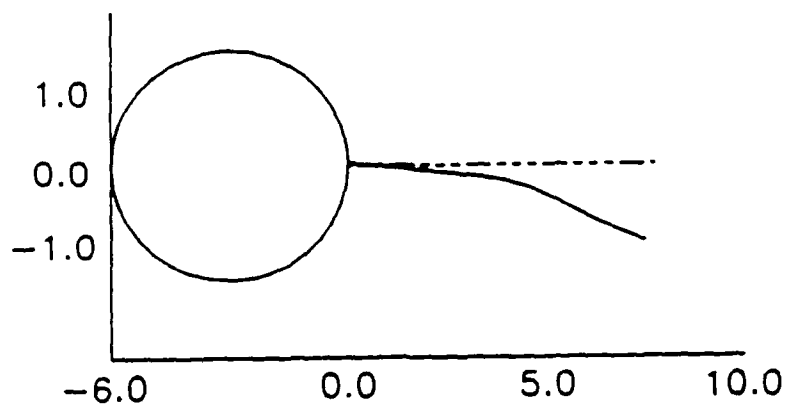
Figure 45. Fin first bending mode Y-Z direction, Frequency = 43 Hz.
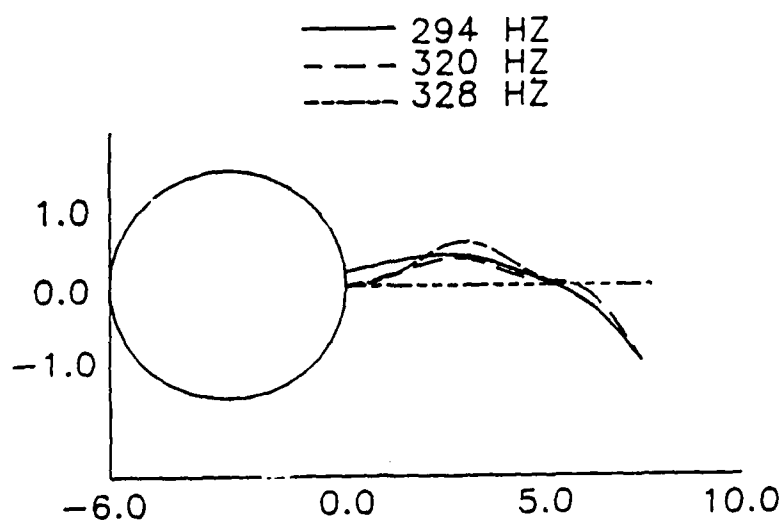
Figure 46. Fin second bending mode Y-Z direction,
Frequency = 294 Hz, 320 Hz, 328 Hz.
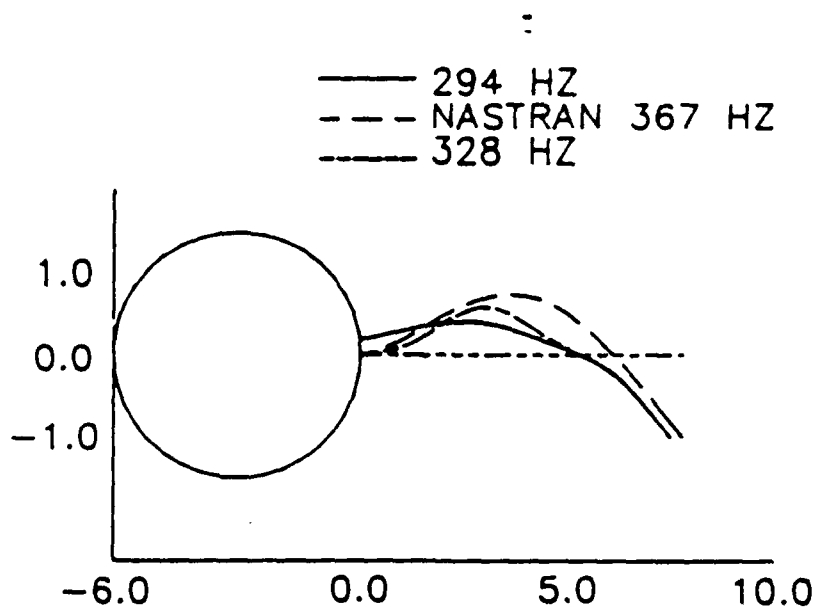
Figure 47. Fin second bending mode in comparison with NASTRAN.
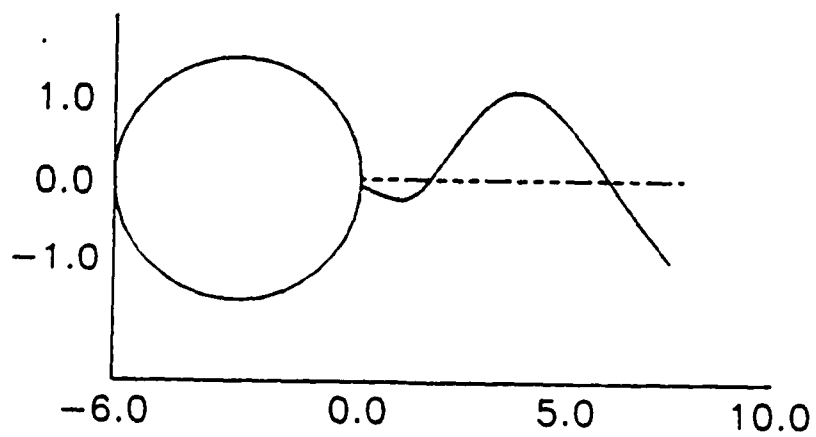
Figure 48. Fin bending mode Frequency = 482 Hz.

61
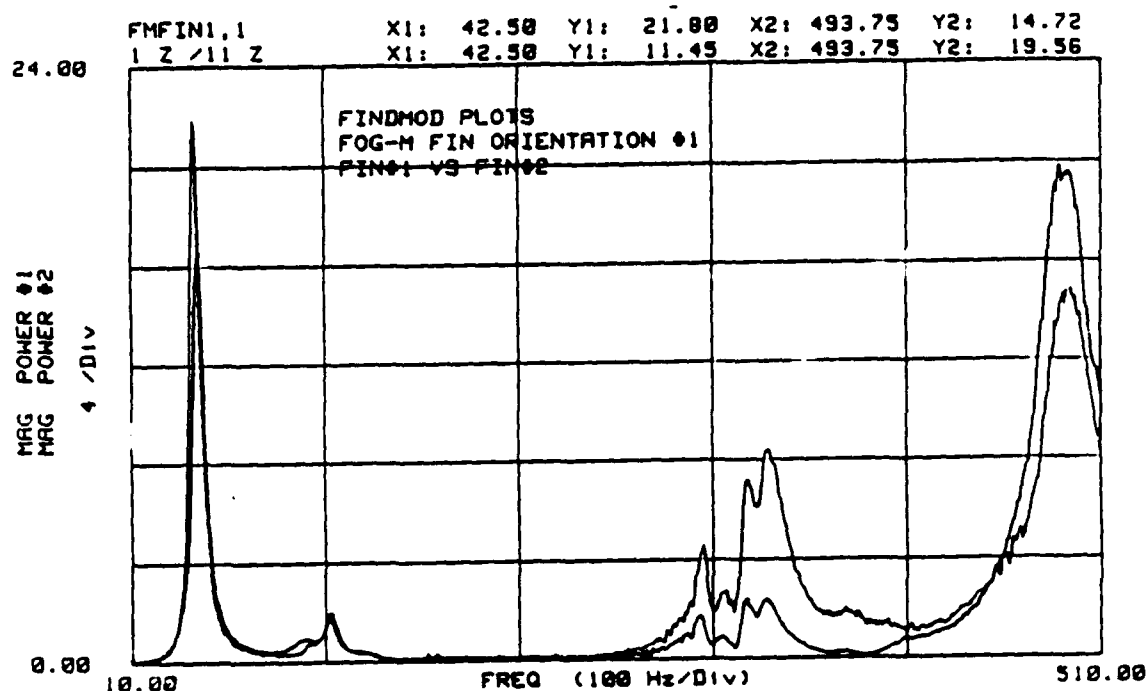
Figure 49. Fin random response function.
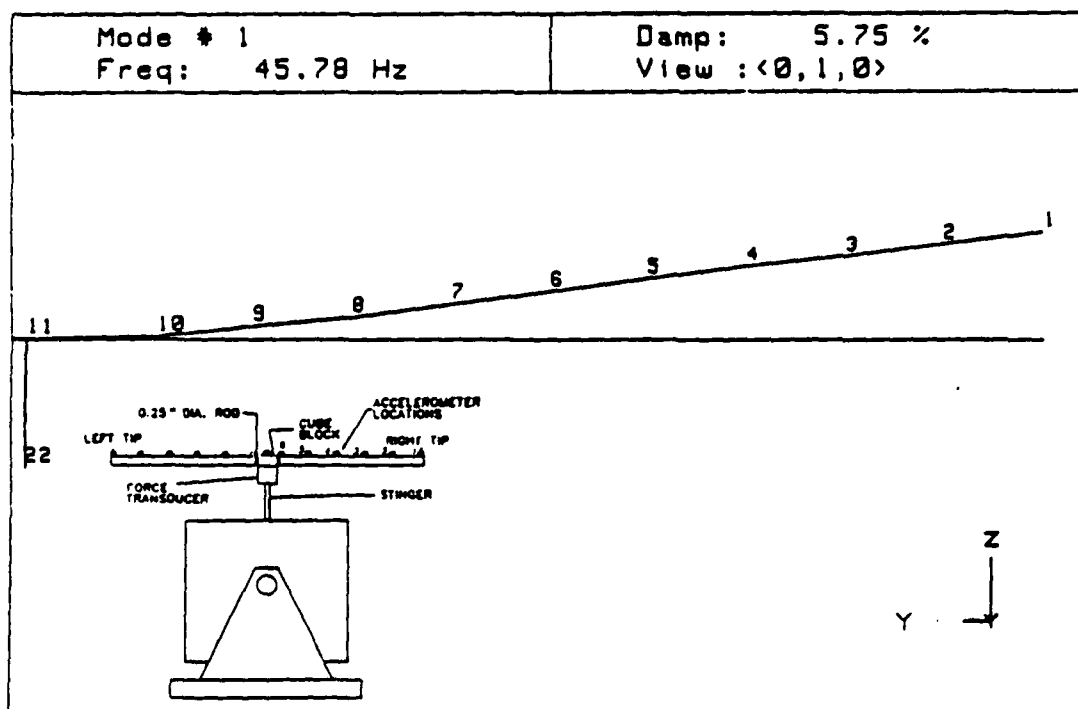
Figure 50. Fin random response first bending mode, Frequency = 46 Hz.
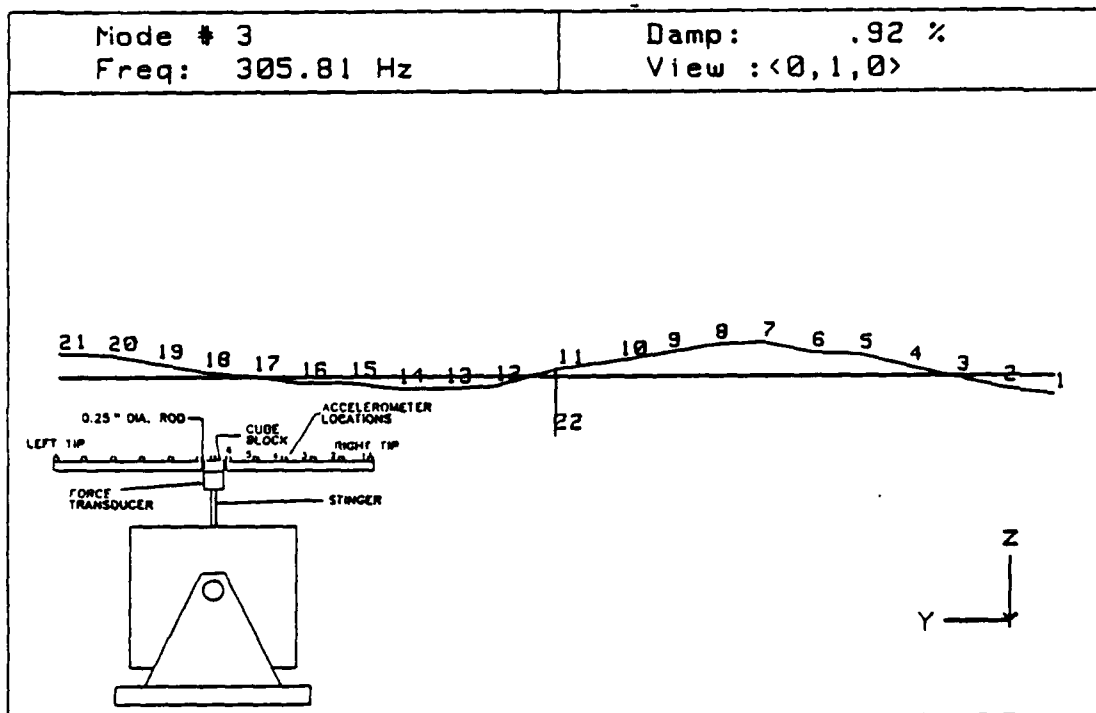
Figure 51.   Fin random response second bending mode, Frequency = 306 Hz.
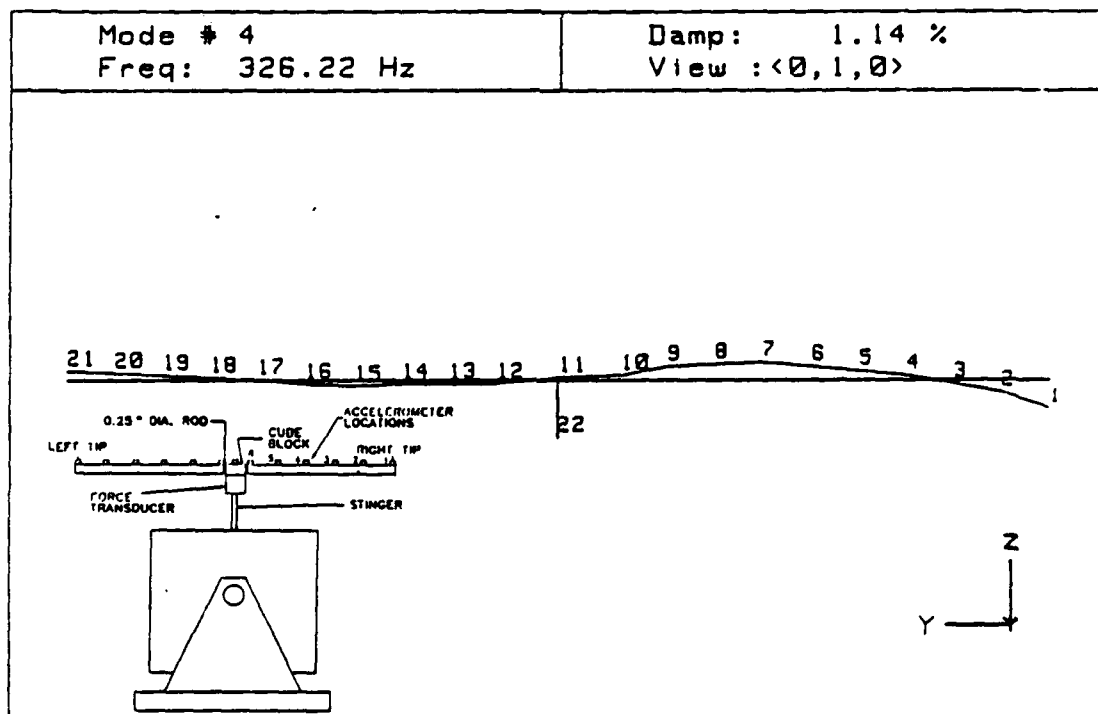
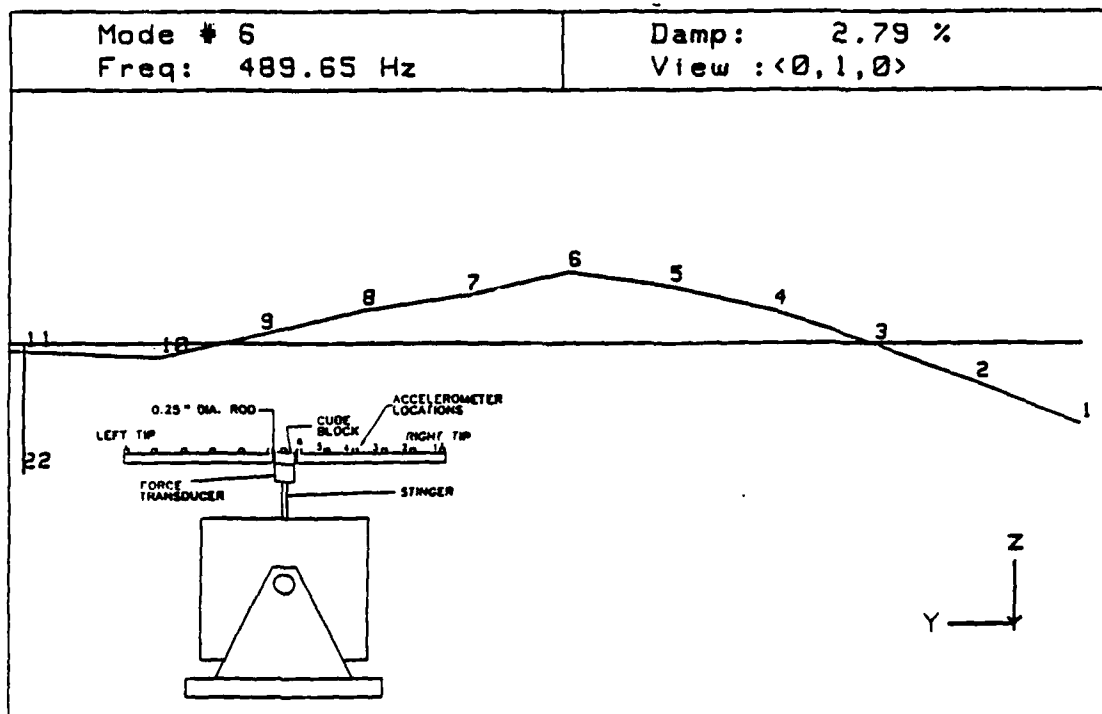Figure 52.   Fin random response second bending mode, Frequency = 326 Hz.

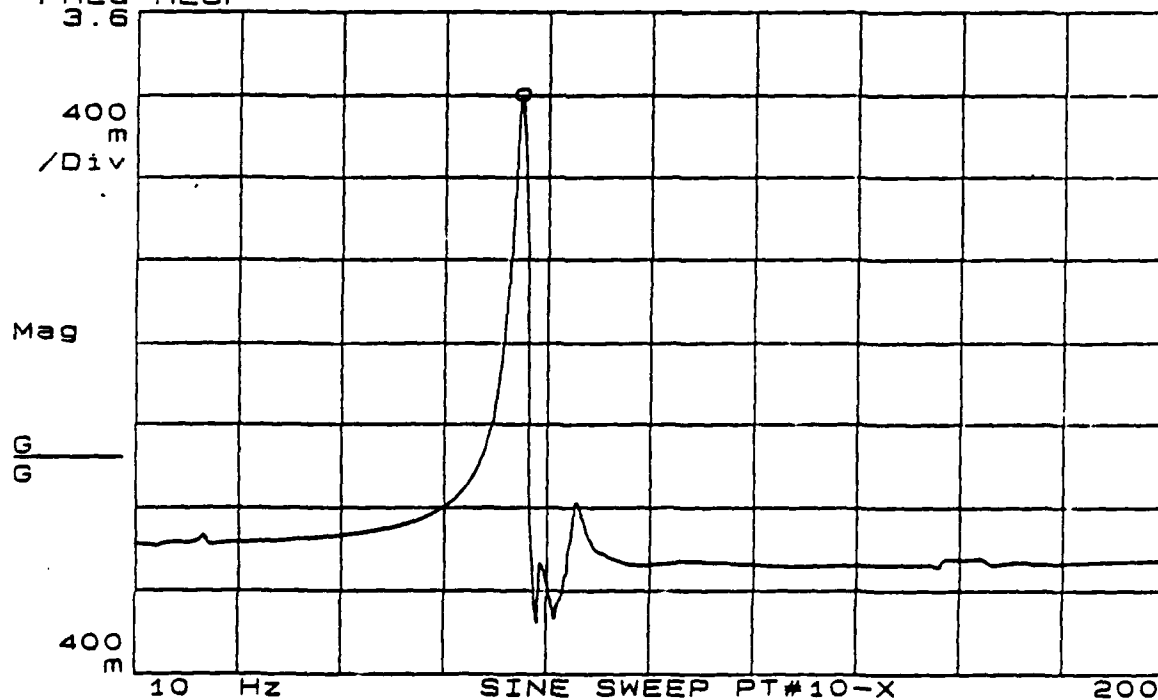Figure 53.   Fin random response Frequency = 491 Hz.
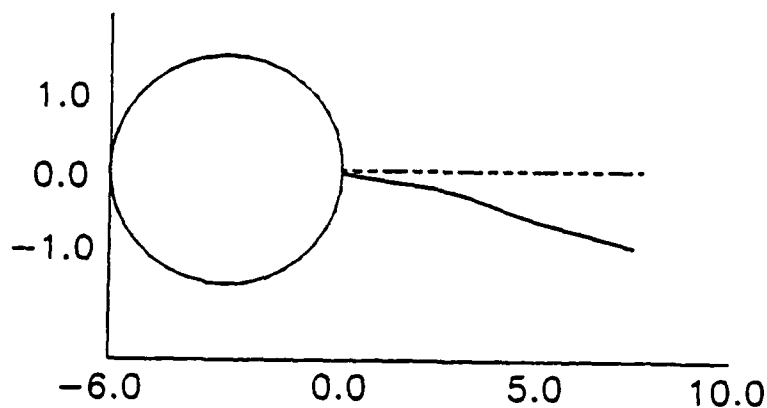

Figure 54.   Fin sine sweep X-direction.

Figure 55. Fin first bending mode X-direction, normal mode method Frequency = 82 Hz.
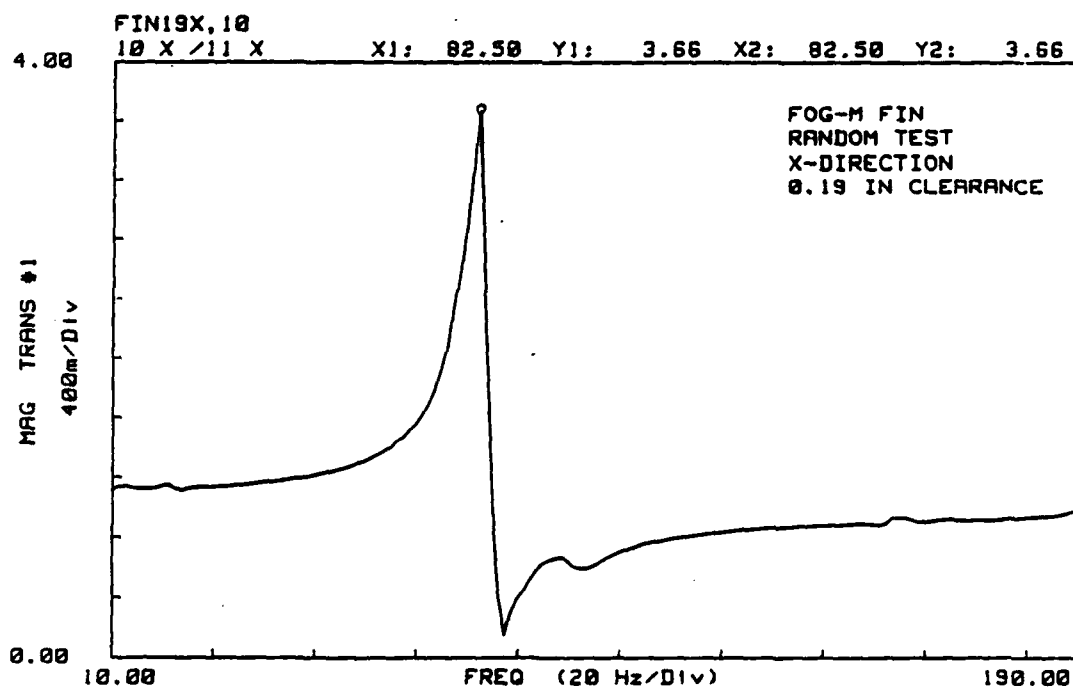

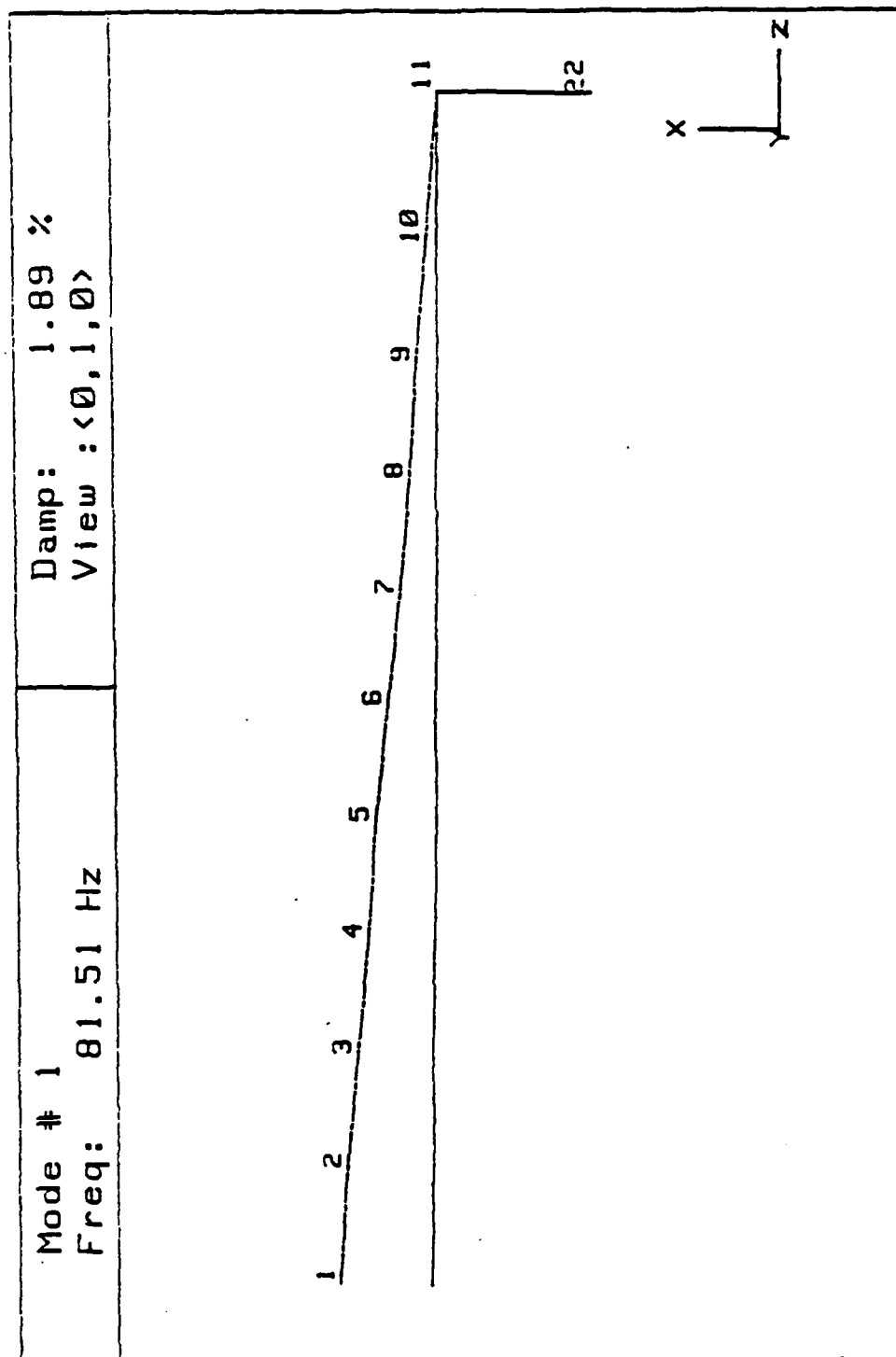Figure 56. Fin random response function X-direction.

65

Figure 57. Fin random response X-direction; first bending mode Frequency = 82 Hz.

REFERENCES

1. Quarterly Technical Review Report, Seeker Development for the FOG-M, Southern Research Institute, 22 October 1987.

2. MIL-STD-810D, Environmental Test Methods and Engineering Guidelines, 19 July 1983.

3. Green, Peter L., Salas, Roque L., Garner, Russell S., and Strickland, H. Eugene, "High Mobility Multi-Wheel Vehicle (HMMWV) FOG-M Modal Survey," Letter Report RD-ST-88-17, 22 February 1988.

DISTRIBUTION LIST

	No. of Copies
AMSMI-RD, Dr. McCorkle	1
Dr. Rhoades	1
-RD-CS-R	15
-RD-CS-T	1
-ST	1
-ST-SA	5
AMCPM-FM	1
AMSMI-SS-AT	1
AMSMI-PR	1
AMSMI-RD-GC-T, Mr. Paul Jacobs	1
-RD-GC-IP, Mr. Fred M. Bush	1
AMSMI-RD-TE/ Mr. Oscar Estrada	1
U.S. Army Materiel System Analysis Activity ATTN: AMXSY-MP Aberdeen Proving Ground, MD 21005	1
ITT Research Institute ATTN: GACIAC 10 W. 35th Street Chicago, IL 60616	1